Dispersion of natural nanomaterials in surface waters for better characterization of their physicochemical properties by AF4-ICP-MS-TEM

Dr. Marco Rinaldi^{1*}, Dr. Ana Lucia Fernández², Dr. Jens Karlsson³

¹Department of Civil Engineering, Politecnico di Milano, Milan, Italy

²Faculty of Environmental Science, Universidad Nacional de Colombia, Bogotá, Colombia

³Department of Environmental Science, Uppsala University, Uppsala, Sweden

Abstract

Characterization and understanding of natural nanomaterials (NNMs) properties is essential to differentiate engineered nanomaterials (ENMs) from NNMs. However, NNMs in environmental samples typically occur as heteroaggregates with other particles, e.g., NNMs, ENMs, and larger particles. Therefore, there is a need to isolate NNMs into their primary particles to better characterize their physicochemical properties. Here, we evaluated the efficiency of sodium hydroxide, sodium oxalate, and sodium pyrophosphate to extract NNMs from surface waters. The extracted NNMs were characterized for total metal concentration by inductively coupled plasma-mass spectrometry (ICP-MS) following full digestion; size distribution, elemental composition and ratios by flow-field flow fractionation (AF4)-ICP-MS; and morphology by transmission electron microscopy (TEM). Sodium pyrophosphate extraction resulted in the highest NNM concentration and the smallest NNM size distribution. Sodium hydroxide and sodium oxalate extraction generated heteroaggregates with a broad size distribution. The NNM extraction efficiency increased with extractant (sodium oxalate and sodium pyrophosphate) concentration. The concentration of metals in the sodium pyrophosphate-extracted NNMs compared to the total metal concentration was elementdependent and varied from as high as >80% for Cu, Zn, and Sr to as low as <5% for Al, Ti, and Nb. This study provides a simple protocol for NNM extraction from complex environmental samples and provides a better understanding of NNM physicochemical properties. The presented NNM extraction protocol forms the basis for ENM extraction from natural waters.

Keywords: Natural nanomaterial; particle extraction; heteroaggregate disaggregation; sodium pyrophosphate; sodium oxalate

1 Introduction

Natural and engineered nanomaterial (NNM, and ENM) detection, quantification and characterization in environmental systems is limited by their heteroaggregation, resulting in their spread over a wide particle size distribution (Labille et al. 2015, Praetorius et al. 2014, Therezien et al. 2014, Wang et al. 2015). Simple filtration (e.g., <100 nm) of natural waters results in the removal of the large majority of NNMs from the nano-fraction, resulting in underestimation of the total NM concentration. The resultant low concentration of NMs hinders their detection, quantification, and characterization by the majority of the nano-analytical techniques. For instance, particle heteroaggregation may limit and/or complicate the applicability of NNM fractionation methods such as asymmetric flow-field flow fractionation (AF4) due to NNM-membrane interactions and/or steric inversion, resulting in poor recovery and/or misleading size distribution information. Similarly, heteroaggregation complicates single particle-inductively coupled plasma-mass spectrometry (sp)-ICP-MS analysis and data interpretation because (i) heteroaggregation could lead to particle sedimentation resulting in underestimation of the total NNM concentration and (ii) it is not possible to differentiate between large particles and aggregates of NNMs of the same composition by (sp)-ICP-MS. Thus, dispersing NNMs from natural heteroaggregates in the form of primary particles is essential to improve NNM characterization by enhancing NNM stability and thus prevent their sedimentation during analysis time, and by increasing NNM concentration and reducing their polydispersity in the fraction of interest (e.g., <100 nm). Dispersing NNM to their primary particle form is likely to facilitate NNM analysis and characterization. A better understanding of inorganic NNM properties (e.g., size, size distribution, elemental composition, and elemental ratios) is essential to differentiate ENMs from NNMs, and thus, to quantify the concentration and distribution of ENMs in environmental systems (Gondikas et al. 2014, Hassellov et al. 2008, Howard 2010, Tiede et al. 2008, Weinberg et al. 2011).

Nanomaterials are defined by the International Organization for Standardization as a material with any external dimension in the nanoscale (1-100 nm) or having internal structure or surface structure in the nanoscale (Boverhof et al. 2015, ISO 2010). Dispersing NNMs from heteroaggregates in environmental samples helps to determine if a material is to be considered as nanomaterial or not based on their primary particle size. Primary NNM size is typically measured by electron and atomic microscopy, which suffers from sample representation and poor statistical power because of the small numbers of NNMs that are typically measured using microscopy techniques (Baalousha and Lead 2013, Sharma et al. 2015, Wigginton et al. 2007). Dispersing NNMs into their primary particles is a prerequisite to enable analysis of NNM primary particle sizes using other - more statistically powerful- analytical techniques such as AF4-ICP-MS and (sp)-ICP-MS (Tuoriniemi et al. 2014, Wagner et al. 2014, Baalousha et al. 2015).

Increasing electrostatic repulsion between NMs within aggregates may break them apart into smaller aggregates and/or into primary particle (Baalousha 2009, Loosli et al. 2013). For instance, adsorption of natural organic matter (NOM) on the surface of iron and titanium oxide micron-sized homoaggregates promoted their disaggregation over a long period of time (e.g., several days) by enhancing inter- and intra-aggregate electrosteric repulsions. Iron oxide aggregates break up first into smaller aggregates and then to primary particles due to attrition mechanisms, whereas titanium dioxide aggregates break up to small aggregates (size > size of primary particle). Increasing electrostatic repulsion between NNM within heteroaggregates by raising the suspension pH using indifferent electrolyte (e.g., sodium hydroxide) was shown to be insufficient to break natural heteroaggregates within a reasonable time frame (e.g., minutes to hours) for further NNM analysis (Regelink et al. 2013). Alternatively, particle dispersing agents such as dithionite, sodium carbonate, sodium pyrophosphate, and sodium oxalate have been shown to disperse iron oxide NNMs and NOM from soils more efficiently than simply

altering the suspension pH using an indifferent electrolyte to enhance electrostatic repulsion by increasing NNM surface charge (Hall et al. 1996, Pronk et al. 2011, Regelink et al. 2014, Tatzber et al. 2007). However, these studies focused on the extraction of iron oxide NNM from soils due to its important environmental functions (Regelink et al. 2013, Schwertfeger et al. 2017), and did not investigate extraction of other NNMs and extraction of aquatic NNMs. Several extraction protocols have been developed to extract NNMs from soils such as sodium chloride, sodium hydroxide, sodium carbonate, sodium pyrophosphate, sodium oxalate, and tetramethylammonium hydroxide (Navratilova et al. 2015, Regelink et al. 2013, Schwertfeger et al. 2017). These extractants have been shown to break natural microaggregates into their smaller constituent aggregates, and thus, increase the concentration of the extracted NNMs in the nano-fraction range (e.g., 1-100) (Lawrence et al. 2015). The extracted NNMs occur typically as aggregates of several NNMs. The presence of such NNM agglomerates complicates the analysis of the extracted particles as discussed above. Furthermore, these extraction protocols are typically applied to extract NNMs from soils and have not been applied for the extraction of aquatic NNMs. Therefore, the aims of this contribution are to (i) evaluate the efficiency of sodium hydroxide, sodium oxalate, and sodium pyrophosphate to disperse and extract NNMs from natural waters, and (ii) determine the physicochemical properties of the primary aquatic NNMs including size, size distribution, morphology, elemental composition and elemental ratios.

2 Materials and methods

2.1 Natural water sampling site

Natural water samples were collected from Stoop Creek and Crane Creek (Columbia, South Carolina, USA) in 1 L high density polyethylene (HDPE) bottles (VWR, USA). All bottles, vials, pipette tips used for sample collection and preparation were acid washed using

10% HNO₃ (Sigma-Aldrich, ACS reagent, USA) by soaking them in acid bath for 48h, then in ultra-pure water (UPW, PURELAB Option-Q, ELGA, UK, R >18 M Ω .cm, T.O.C. <2 ppb) bath for 48 h. All sampling bottles were rinsed three times with the natural water prior filling the bottles by submerging them in the water to avoid presence of air and then stored at 4°C.

2.2 Chemicals and reagents

Sodium pyrophosphate (NaPP, Alfa Aesar, Analytical grade, Japan) and sodium oxalate (NaOx, Alfa Aesar, Analytical grade, China) stock solutions were prepared at 100 mM and pH 10 in UPW water. NaOH (VWR Analytical, BDH®, ACS, USA) was used to adjust samples' pH. The pH of all samples was routinely monitored using a pH meter (Mettler Toledo, FiveEasy, Switzerland) and adjusted to 10 as necessary using NaOH solution.

2.3 Nanomaterials extraction from natural waters

A 36 mL aliquot of the natural water was transferred into a 50 mL polypropylene centrifuge tube (Eppendorf, Mexico). Aliquots of NaPP, NaOx stock solutions and UPW were added to the natural water sample to reach NaPP and NaOx concentrations of 0 (only UPW added), 2 and 10 mM (typical range of concentration for metal oxides extraction particle in soils (Regelink et al. 2013) and a final mixture volume of 40 mL. pH was then adjusted to 10 using NaOH to enhance natural heteroaggregate disaggregation by electrostatic repulsion (Baalousha 2009). Samples were stirred in a tube rotator at 30 rpm (Fisher Scientific, China) overnight, and then sonicated for 60 min in a sonication bath (Branson, 2800, 40 kHz, Mexico) to enhance NNM dispersion. Samples were then centrifuged (Eppendorf, 5810 R, Germany) at 3,100× g for 120 min to remove particles larger than 100 nm based on intrinsic centrifuge characteristics, a particle density of 2.5 and Stokes' law calculation (Tang et al. 2009). The top 30 mL of supernatant was collected and stored at 4°C for further analysis.

2.4 Total water digestion for total elemental analysis by ICP-MS

The bulk water and the extracted NNM suspensions were digested in 15 mL Teflon vessels (Savillex, USA) on custom-made Teflon covered hotplates placed in a box equipped with double-HEPA filtered forced air in a metal-free HEPA filtered air clean lab at the Center for Elemental Mass Spectrometry, University of South Carolina. A 10 mL aliquots of bulk water and extracted NNM suspensions were placed in the vessel and weighted (Mettler Toledo, Excellence Plus, Switzerland). Samples were dried down at 110°C and treated with 1 mL of 30% H₂O₂ (Fisher Chemical, USA) for 2 h at 70°C to remove organic matter. H₂O₂ was evaporated and the sample was digested with 2 mL of HF: HNO₃ (3:1) mixture (Teflon suboiling distilled.) for 24 h at 110°C to dissolve silicates, carbonates, and metal oxides. After evaporation of the acid mixture at 110°C, the residue was repeatedly attacked with 1 mL of Teflon-distilled HNO₃ to break up insoluble fluoride salt that may have formed during the sample digestion, and HNO₃ was left to evaporate at 110°C. The dried sample was subsequently redissolved in 5 mL of 2 % HNO₃ with the aid of sonication and heating to 50°C. The solutions were transferred to 15 mL polypropylene centrifuge tubes (Eppendorf, Mexico) and stored at 4°C. All samples were centrifuged (Eppendorf, 5810 R, Germany) for 5 min at 3,100× g prior ICP-MS analysis to remove any refractory material and to prevent clogging of the introduction system.

Elemental concentrations of the digested NNM suspensions were determined on a Thermo Fisher ELEMENT 2 high resolution-inductively coupled plasma-mass spectroscopy (HR-ICP-MS) at the Center for Elemental Mass Spectrometry, University of South Carolina. Samples were injected to the ICP-MS using 100 μL min⁻¹ PFA nebulizer (~120-150 μL min⁻¹ actual uptake) in self aspiration mode and a quartz cyclonic spray chamber. The isotopes measured were ⁷Li, ²⁷Al, ⁴⁵Sc, ⁴⁷Ti, ⁵¹V, ⁵³Cr, ⁵⁵Mn, ⁵⁷Fe, ⁵⁹Co, ⁶⁰Ni, ⁶³Cu, ⁶⁶Zn, ⁶⁹Ga, ⁸⁵Rb, ⁸⁸Sr, ⁸⁹Y, ⁹⁰Zr, ⁹³Nb, ¹⁰⁷Ag, ¹¹¹Cd, ¹¹⁵In, ¹¹⁸Sn, ¹³³Cs, ¹³⁸Ba, ¹³⁹La, ¹⁴⁰Ce, ¹⁴¹Pr, ¹⁴⁶Nd, ¹⁴⁹Sm, ¹⁵¹Eu, ¹⁵⁷Gd, ¹⁵⁹Tb,

¹⁶³Dy, ¹⁶⁵Ho, ¹⁶⁷Er, ¹⁶⁹Tm, ¹⁷³Yb, ¹⁷⁵Lu, ¹⁷⁸Hf, ¹⁸¹Ta, ²⁰⁸Pb, ²³²Th and ²³⁸U. Isotopes with potential isobaric interferences (*e.g.*, Al, Ca, Co, Cr, Cu, Fe, Ga, Mg, Mn, Ni, Ti, V, and Zn) were measured in medium resolution (m/Δm = 4000) to resolve such interferences, while the other elements were measured in low resolution for maximum sensitivity (m/Δm = 300). Concentrations were calculated against a multi-element standard solution composed by a mixture of IV-ICPMS-71A (ICP-MS Complete Standard, Inorganic Ventures, USA) and ICP-MS-68A-B (68 Element Standard, High-Purity Standards, USA) multi-element standards.

The elemental concentrations of the USGS reference materials BCR-2 and BIR -1 basalts run as unknowns after digestion following the digestion procedure described above demonstrate high recovery (approximately 100%), precision (2-3%) and accuracy of our method (*e.g.*, better than 5% for most elements) (Loosli et al. 2019).

2.5 AF4-ICP-MS

Elemental based size distributions were measured by AF4-ICP-MS by coupling Wyatt AF4 (DualTec Eclipse, Wyatt Technology, USA) with a NexION350D (Perkin Elmer, USA) quadrupole ICP-MS. All separation experiments on AF4 used a 1 kDa molecular weight cut-off polyethersulfone membrane (Pall Corporation, USA) and a 350 μm spacer. Carrier solution consisted of 10 mM NaNO₃ (VWR Analytical, BDH[®], ACS, Canada) at pH 10. Injection volume was 900 μL, with 10 min focus time. The detector flow rate was set to 1.0 mL min⁻¹, while two kinds of gradient cross flow were applied: gradient cross flow declining from 2.5 mL min⁻¹ to 0.0 mL min⁻¹ over 45 min of elution; and gradient cross flow declining from 4.0 mL min⁻¹ to 0.0 mL min⁻¹ over 120 min of elution. Latex Nanosphere size standards of 20, 40, 80, and 150 nm (Thermo Scientific, USA) were used to calibrate the AF4 channel and to establish the relationship between particle hydrodynamic diameter and retention time. It is worth noting here that the Latex Nanosphere size standards particles might have a different surface charge

and different shape than NNMs, which may affect the accuracy of the measured hydrodynamic diameters (Dubascoux et al. 2008, Loeschner et al. 2013).

Dissolved multi-element standards mixture of IV-ICPMS-71A (ICP-MS Complete Standard, Inorganic Ventures, USA) and ICP-MS-68A-B (68 Element Standard, High-Purity Standards, USA) were used for the ICP-MS mass concentration calibration ranging from 0.1 to 100 μg L⁻¹ before coupling AF4 to ICP-MS. Samples were introduced to the ICP-MS using a T-junction to monitor internal standards (ICP Internal Element Group Calibration Standard, BDH Chemicals, USA) for quality control and to acidify (1% HNO₃ after mixing with the sample) the samples just prior introduction into the ICP-MS in order to avoid particle stability changes. A 50 ms dwell time was applied for all the measured analytes. NNM recovery in AF4-ICP-MS varied between 40 and 80%.

2.6 Transmission electron microscopy

Morphology and elemental analysis of particles in the bulk water and the extracted NNM suspensions were performed by Transmission Electron Microscope (TEM). TEM samples were prepared using the drop deposition method according to the procedure described elsewhere (Prasad et al., 2015). TEM grids were functionalized using a positively charged Polyt-L-Lysine (1% w/v in water solution; Ted Pella, USA) to enhance the attachment of the negatively charged colloids on the grid surface. Poly-L-lysine (10 μL) was deposited on a 300 mesh Cu grid (Ted Pella, Pelco[®], USA) for 20 min followed by rinsing three consecutive times in UPW to remove excess poly-L-lysine. Subsequently, a 20 μL of extracted NNM suspensions was deposited on the poly-L-lysine functionalized TEM grids for 15 min. The excess water was removed using a filter paper and the TEM grids were rinsed three times using UPW to prevent salt crystallization and NM aggregation during the drying process. The TEM grids were then left to dry for 12 h in a covered petri dish to avoid atmospheric particle deposition. Microscopy

analysis were performed in a LaB₆ Jeol 2100 TEM, operated at 200 keV and equipped with a Jeol EX-230 Silicon Drift Detector with a 60 mm² window of acquisition for energy dispersive X-ray (X-EDS) analysis of elements. Micrographs were acquired at different magnifications, ranging from $500 \times$ to $400,000 \times$, to gather information about the NNM size and morphology.

3 Results and discussion

1

2

3

4

5

6

7

8

9

10

11

12

13

14

15

16

17

18

3.1 Properties of bulk natural waters

The Stoop Creek (SC) water is generally characterized by higher elemental concentrations than those measured in Crane Creek (CC) water (Table S1). The higher Al, Fe, Ti, and Ce concentrations (>10 folds) in SC water compared to CC water indicates the higher concentration of suspended particulate matter, and potentially NNM, such as clay particles, iron oxides, titanium dioxides, and cerium oxides in SC water than those in CC water. TEM analysis of bulk SC water illustrates that particles (NNMs, colloids and micron-sized particles) occur as compact aggregates together with fibril network of natural organic matter (Figure 1a). Figure 1a and b show an aggregate of nearly spherical silica particles (light contrast) and smaller spheroid iron oxide (dark contrast). The majority of inorganic colloids in surface waters are aluminosilicates (clays), silica, and iron oxide particle (Buffle and Leppard 1995). Whereas most clays are sheetlike angular particles, silica and iron oxide particle have irregular but nearly spherical shape as observed in Figure 1. NOM plays an important role in determining the stability of inorganic particles in natural water. Whereas globular compounds - such as fulvic acids humic acids enhance the stability of particles in the aquatic environment due to electrosteric effects; large semi flexible and rigid biopolymers destabilize particle suspensions via polymer bridging mechanisms (Buffle et al. 1998, Wilkinson et al. 1997).

3.2 Effect of extractants on metal concentration in the extracted NNM suspensions

20

21

22

23

24

25

26

27

28

29

30

31

32

33

34

35

36

37

38

39

40

41

42

43

The elemental concentration in the extracted NNM suspensions are presented in Table S2. Overall, the elemental concentrations in the extracted NNM suspensions increased following the order 0.1 mM NaOH < 2 mM NaOx < 10 mM NaOx < 2 mM NaPP < 10 mM NaPP for both SC and CC waters. Additionally, for the same extractant, the elemental concentrations in the SC extracted NNM suspensions are higher (up to 40 folds) than those measured in the CC extracted NNM suspensions, in good agreement with the higher total elemental concentrations in SC water than those measured in CC water (Table S1). The percentage (%) of element concentrations in the extracted NNM suspensions compared to the total metal concentration in the bulk water for NaOH- (control protocol), NaOx-, and NaPPextracted NNMs are presented in Figure 2. The % of element concentrations in the 0.1 mM NaOH-extracted NNM suspensions is low (< 3%) for most elements, especially for clayforming elements (e.g., Al, Fe, and Ti), indicating a low NNM extraction efficiency. The % elemental concentration of some element (e.g., Cu, Sn and Sr) in the 0.1 mM NaOH-extracted NNM suspensions was higher (> 20%), indicating higher extractability of these elements compared to clay forming elements. The extraction behavior of elements is in agreement with their mobility in the natural environment. Elements such as titanium, niobium, tantalum, zirconium, and aluminum are highly immobile, whereas elements such as rubidium and strontium are highly mobile in the environment (Holland and Turekian 2010). Thus, alkaline pH, i.e. 0.1 mM NaOH results in the extraction of only a small fraction of metals and NNMs from aquatic samples, in good agreement with previous studies on iron oxide NNM extraction from soils (Regelink et al. 2013, Tang et al. 2009). This is due to the limited release of NOM from natural microaggregates and to the release of divalent cations (e.g., Ca²⁺, Mg²⁺, etc) during extraction. The release of divalent cations may compromise NNM extraction by destabilizing NNMs via surface charge screening and NOM bridging (Jolivet 2000, Philippe and Schaumann 2014).

45

46

47

48

49

50

51

52

53

54

55

56

57

58

59

60

61

62

63

64

65

66

67

68

For a given element, the % of element concentrations in the extracted NNMs increase following the order NaOH < NaOx < NaPP (Figure 2a and b). This is likely due to the disaggregation of natural heteroaggregates into smaller aggregates (e.g., < 200 nm, see discussion in section 3.3). The ability of oxalate and pyrophosphate to disperse NNM can be attributed to two different mechanisms. First, oxalate and pyrophosphate can displace NOM from the surface of NNMs and enhance NNM surface charge due to their higher charge density compared to NOM (Driver and Perdue 2014, Simoes et al. 2017). The adsorption of oxalate and pyrophosphate on NNM surfaces enhance inter and intra NNM electrostatic repulsions, and ultimately induce NNM disaggregation (Jolivet 2000, Pansu and Gautheyrou 2006). Second, oxalate and pyrophosphate are metal chelators, which sequester metal ions, thus reducing free multivalent ion concentration in the extracted NNM suspensions. This in turn, reduces the screening of NNM surface charge by removing multivalent cations from solution and reduces NNM aggregation via bridging mechanism (Philippe and Schaumann 2014) and/or multivalent cation specific adsorption (Jolivet 2000). The higher efficacy of NaPP compared to NaOx in dispersing NNM from natural heteroaggregates can be attributed to the higher pyrophosphate adsorption affinity to NNM surfaces (e.g., clays, iron oxides, titanium dioxide, and cerium oxides) (Doetterl et al. 2015, Connor and McQuillan 1999, Loosli et al. 2018, Arai and Dahle 2018) and to multivalent cations (Furia 1972, Huang and Sumner 2011) than oxalate, and the higher ability of pyrophosphate to displace NOM from the surfaces of NNMs compared to oxalate (He et al. 1999).

The % element concentrations in the NaOx- and NaPP-extracted NNM suspensions increase with the increase in extractant concentrations (Figure 2a and b) within the extractant concentration range used in this study. Figure 3 shows the elemental concentration factor; that is the concentration of the NaOx- and NaPP-extracted metals compared to the control extraction (0.1 mM NaOH). The element concentrations in 2 mM NaPP-extracted SC NNM suspension

were 12 folds higher than those of the 0.1 mM NaOH treated SC water, while 10 mM NaPP extraction provides 17 times higher concentrations than 0.1 mM NaOH. Similar for CC waters, 2 mM NaPP-extracted NNM suspension has 21 times higher element concentrations than 0.1 mM NaOH, and 10 mM NaPP increases the difference to 31 folds. For NNM extracted with NaOx the element concentrations in SC NNM suspension 5 folds higher than those of the 0.1 mM NaOH treated SC water. For CC waters, 2 mM NaOx-extracted NNM suspension has 6 times higher element concentrations than 0.1 mM NaOH, and 10 mM NaOx increases the difference to 9 folds.

The higher % metal concentration in the extracted NNM suspensions compared to the bulk water (Figure 2b) and the higher metal concentration factor compared to the control extraction (Figure 3b) for CC water compared to those for SC water (Figure 2a and 3a) may be attributed to the lower total metal, and thus NNM, concentrations in CC compared to SC. Higher extractant to NNM concentration ratio enhances NNM recovery as discussed above. Additionally, the characteristics (e.g., composition, concentration, size distribution, etc.) of the suspended particulate matter also vary from one water to another, which may have a significant impact on NNM extraction efficiency. Therefore, the measured metal, and thus NNM, concentrations in the extracted NNM suspensions do not represent the total metal, and thus NNM, concentrations in the bulk samples. Consequently, measuring total metal concentration in bulk waters is required to estimate the total NNM concentrations and to evaluate and optimize the NNM extraction efficiency. Nonetheless, reducing NNM dispersity and increasing their concentration in the extracted suspensions compared to the bulk water facilitates and simplify further NNM characterization (e.g., size, size distribution, elemental ratios, etc.) by ca. AF4-ICP-MS and TEM as discussed below.

3.3 Effect of extractant on NNM size distribution

94

95

96

97

98

99

100

101

102

103

104

105

106

107

108

109

110

111

112

113

114

115

116

117

The elemental based-size distribution and elemental ratios as a function of particle size of the extracted NNMs were determined by AF4-ICP-MS. AF4 fractograms for a select set of metals such as Mn (ubiquitous in soils and sediments and affect groundwater composition (Post 1999)), Ce (most common lanthanide) and, Pb (toxic metal present in the environment due to its wide spread presence, mainly as oxides, as a component of lead paint and as naturally occurring minerals (Baltrusaitis et al. 2012)) are presented in Figure 4. These elements were selected because they were present in the water samples at sufficiently high concentrations to obtain decent AF4 signal. Mn, Ce, Pb exhibit a broad size distribution for NaOH-extracted NNMs (Figure 4a), and the majority of these metals elute at the end of the run indicating that these metals occur mainly as large NNMs, or as heteroaggregates (>100 nm) of small NNMs. The modal hydrodynamic diameter (~150 nm) of NaOH-extracted NNMs is higher than the theoretical cut-off applied for the fractionation by centrifugation, which can be attributed to the presence of plate shape clay particles and/or porous fractal NNM heteroaggregates, which have significant implication on NNM separation by centrifugation and NNM behavior in the AF4 channel. For instance, fractal NNM heteroaggregates may have density lower than the hard sphere density assumed in Stocks' equation ($\rho = 2.5 \text{ g cm}^{-3}$) used to calculate NNM size cutoff for the separation of NNM by centrifugation, which increases the apparent size cut-off of the extracted NNMs (Baalousha and Lead 2007). Finally, the equivalent hydrodynamic diameter obtained by AF4 is calculated based on AF4 channel calibration using spherical polystyrene standards which may not behave/diffuse similar to NNMs and their heteroaggregates in the AF4 channel (Baalousha et al. 2005). The diffusion of platelets and porous aggregate deviates from the theoretical diffusion of hard spherical particles assumed in FFF theory (Baalousha et al. 2011). NNM aggregates are often irregular and fractal/porous (Leppard et al. 1986, Wilkinson et al. 1999), they can exhibit lower diffusion coefficient compared to hard spheres (Dubascoux et al. 2008).

The 2 mM NaOx-extracted NNMs (Figure 4b) show a broad size distribution with higher concentration of metals at all sizes in comparison to those measured for NaOH-extracted NNMs. However, a large fraction of metals also elutes at the end of the AF4 run. This indicates that the 2 mM extracted-NNMs are a mixture of NNM heteroaggregates of different sizes including a significant proportion of heteroaggregates with a hydrodynamic diameter >100 nm. For 10 mM NaOx-extracted NNMs (Figure 4c), Mn, Ce and Pb concentrations increase for small hydrodynamic diameters and decrease for larger hydrodynamic diameters, indicating the disaggregation of natural heteroaggregates and the increased concentration of primary NNMs, and small NNM heteroaggregates (*e.g.*, <100 nm). Overall, these results suggest that the concentration of the extracted NNMs increases with the increase in NaOx concentration, in good agreement with the increase in the total metal concentrations in the extracted NNMs with the increase in NaOx concentration as discussed above.

The 2 mM NaPP-extracted NNMs (Figure 4d) show a narrower size distribution and higher elemental concentrations compared to NaOH- and NaOx-extracted NNMs with a mode value ~8 nm, together with the elution of some NNM aggregates (>150 nm) at the end of the AF4 run, indicating the presence of a small fraction of NNM heteroaggregates. At 10 mM NaPP (Figure 4e), the extracted NNM size distribution is even narrower than the size of the 2 mM NaPP-extracted NNMs, together with higher elemental concentrations at smaller sizes and the absence of any large aggregated materials at the end of the AF4 run and. These results indicate a more efficient disaggregation of NNM heteroaggregates and higher NNM extraction using NaPP, in particular at the higher NaPP (10 mM) concentration.

The size distribution of Ce, Mn, and Pb rich particles for the CC water are presented in Figure S1. The elemental size distribution (NaPP < NaOx < NaOH) and concentration (NaPP > NaOx > NaOH) follow the same trends as those reported for SC water. Element size distribution of NNMs for SC and CC waters for other elements (Al, Ag, Co, Fe, La, Eu, Er, Cu

and V) are presented in Figures S2 and S3. These elemental size distributions follow the same size distribution trends as Ce, Mn, and Pb except for Al. The majority of the extracted Al-rich NNMs have a similar size distribution, with broad size distribution and aggregates >100, regardless of the extraction agent. This behavior can be attributed to the dominance of Al in platelet clay and muscovite particles and to the high concentration of Al-containing NNMs, which may limit the disaggregation of clay particles due to the effect of extractant/NNM ratio.

TEM analyses show that NaOH-extracted NNMs occur mainly as aggregates of NNMs and NOM (Figure 5a); NaOx-extracted NNMs occur as primary NNMs and aggregates of NNMs and NOM (Figure 5b); and NaPP-extracted NNMs occur predominantly as primary particles (Figure 5c). These TEM results are in good agreement with the extracted NNM size distributions obtained by AF4-ICP-MS with lower modal size and narrower size distribution for NNMs extracted with NaPP.

3.4 Elemental associations and ratios

Quantifying elemental ratio of elements forming NNMs is essential to understand element associations and to quantify the concentration of anthropogenic particles in environmental systems. For instance, Rare Earth Element ratios (REE; i.e. Ce/La, Ce/Nd, Ce/Pr) are typically used as geological tracers to determine trace metal-natural colloids association and can be used to asses anthropogenic input of cerium oxide particles into the environment (Montano et al. 2014, Neubauer et al. 2013). Elemental ratios of Ti with Al, V, Ga, Y, Nb, Eu, Ho, Er, Tm, Yb and Ta have been proposed to evaluate the anthropogenic input of TiO₂ ENMs to the environment (Gondikas et al. 2014). However, natural background ratios and the relationship between NNM size and elemental ratios is not yet well established.

Elemental ratios were calculated for the bulk waters and extracted NNMs following full digestion as well as for the fractionated NNMs by AF4-ICP-MS. The Zr/Hf ratio was

168

169

170

171

172

173

174

175

176

177

178

179

180

181

182

183

184

185

186

187

188

189

190

191

constant for both bulk waters (Table S3) and for the extracted NNM suspensions (Figure 6a) for the different extraction protocols with an average ratio of 29.7 ± 3.0 in good agreement with literature (Hui et al. 2011). The constant Zr/Hf ratio indicates the absence of anthropogenic Zr and Hf and the reliability of sample digestion and analysis by ICP-MS (Liu et al. 2014). Ce/La, Ce/Nd and Ce/Pr were similar in SC and CC waters with ratios equal to 2.2 ± 0.1 , 2.5 ± 0.1 and to 9.8 ± 0.3 , respectively (Figure 6b and c). The Ce/La ratio is similar to the average Earth Ce/La crustal value, indicating the absence of anthropogenic sources of cerium oxide particles in these waters (Lide 2008). Ce/REE ratios in the extracted NNM suspensions are similar to those calculated for the bulk water and these ratios are independent of the extraction procedure, indicating that the extracted NNMs have the same elemental ratios as those of larger particles. Ti/Nb is slightly higher in SC bulk water than in CC bulk water (383 and 349, respectively) and both of these ratios are higher than the average continental crust value of 320, which may be attributed to anthropogenic input of TiO₂ ENMs (Table S1) into SC and CC waters (Gondikas et al. 2014, Loosli et al. 2019). Further research is required to evaluate the natural background ratio of Ti/Nb in natural waters and to validate the use of Ti/Nb elemental ratio to estimate TiO₂ ENM concentrations, and to determine the potential sources of these TiO₂ ENMs in surface waters.

For the 0.1 mM NaOH-, 2 mM NaOx-, and 10 mM NaOx-extracted NNMs, the Ce/La ratio is high with high fluctuations at small sizes and decrease to lower values at larger sizes (Figure S5). This is because CeO₂ NNMs occur as heteroaggregates in 0.1 mM NaOH-, 2 mM NaOx-, and 10 mM NaOx-extracted NNMs and they elute at the end of the AF4 run. For the 2mM NaPP- and 10 mM NaPP-extracted NNMs, the Ce/La ratio is lower than those calculated for the 0.1 mM NaOH-, 2 mM NaOx-, and 10 mM NaOx-extracted NNMs at small sizes due to the disaggregation of natural NNM heteroaggregates and the elution of the majority of CeO₂ ENMs at small sizes. This in turn improves the detectability of Ce and La and thus reduces the

fluctuation in the Ce/La ratio, and ultimately improves the probability of detecting and quantifying ENM concentrations based on the increase in the elemental ratios due to the introduction of pure ENMs.

Size-based elemental ratios obtained by AF4-ICP-MS may provide further understanding of the elemental associations within NNMs, and may facilitate the detection of ENMs in natural sample. Disaggregating heteroaggregates and releasing of NNMs and/or ENMs in their primary particles form may result in a high concentration of ENMs within a narrow size range, which will enhance any shift in the elemental ratios within that size range compared to natural elemental ratio. An increase of the elemental ratios, i.e. Ce/La, through the size distribution indicates the presence of CeO₂ ENMs. In the samples investigated in this study, Ce/La was constant throughout the NNM size distribution indicating the absence of CeO₂ contamination in these samples (Figures S5 and S6).

4 Conclusion and Outlook

This contribution presents an approach to extract NNMs (which can also be applied to extract ENMs) from surface waters mainly in their primary particle form. Sodium pyrophosphate extracts the highest concentration of NNMs in their primary particle form, whereas sodium oxalate and sodium hydroxide extract lower concentration of NNMs in the form of small heteroaggregates. Dispersion of NNMs into their primary particles and the increased elemental concentrations in the extracted NNM suspensions enabled the identification and characterization (*e.g.*, size distribution, elemental composition and elemental ratios) of the different NNM phases using AF4-ICP-MS. Therefore, the presented NNM extraction approach will likely improve the probability of detecting and quantifying metal-based ENMs in environmental samples based on their elemental composition and elemental ratios. The presented approach also will improve the understanding of NNM environmental

functions such as the role of NNMs in the partitioning of metal contamination among the different phases *e.g.*, bulk and colloidal phases, and the environmental fate and transport of contaminants with strong affinity to NNMs. The occurrence of a significant extractable fractions of NNMs in natural heteroaggregates may infer that these NNMs play a major role in the occurrence of trace metal contamination in the particulate phase.

It is worth noting here that the use of reactive extraction agents such as sodium pyrophosphate might result in transformation of NNM *e.g.* by dissolution or phase transformation, which should be considered in future studied. Nonetheless, our results indicate that these transformations, if occurred, did not influence the elemental ratios of strongly associated elements such Zr/Hf and Ce/La.

Acknowledgments

The authors are grateful to the financial support received from the NSF CAREER award (1553909) to Dr. Mohammed Baalousha, the Swiss National Foundation (P2GEP2_165046) to Dr. Frédéric Loosli, and the China Scholarship Council (CSC_201606380069) to Zebang Yi. We thank Dr. Michael Bizimis for providing access to the clean lab facilities at the Center for Elemental Mass Spectrometry, School of Earth and Ocean Sciences at the University of South Carolina. This work was supported by the Virginia Tech National Center for Earth and Environmental Nanotechnology Infrastructure (NanoEarth), a member of the National Nanotechnology Coordinated Infrastructure (NNCI), supported by NSF (ECCS 1542100).

References

Arai, J. and Dahle, J.T. (2018) Redox-ligand controlled chemical fate of ceria nanoparticles in an agricultural soil. Journal of Agricultural and Food Chemistry 66, 6646-6653.

Baalousha, M. (2009) Aggregation and disaggregation of iron oxide nanoparticles: Influence of particle concentration, pH and natural organic matter. Science of the Total Environment 407(6), 2093-2101.

Baalousha, M., Kammer, F.V.D., Motelica-Heino, M. and Le Coustumer, P. (2005) 3D characterization of natural colloids by FIFFF-MALLS-TEM. Analytical and Bioanalytical Chemistry 383(4), 549-556.

Baalousha, M. and Lead, J.R. (2007) Size fractionation and characterization of natural aquatic colloids and nanoparticles. Science of the Total Environment 386(1-3), 93-102.

Baalousha, M. and Lead, J.R. (2013) Characterization of natural and manufactured nanoparticles by atomic force microscopy: Effect of analysis mode, environment and sample preparation. Colloids and Surfaces a-Physicochemical and Engineering Aspects 419, 238-247.

Baalousha, M., Stolpe, B. and Lead, J.R. (2011) Flow field-flow fractionation for the analysis and characterization of natural colloids and manufactured nanoparticles in environmental systems: A critical review. Journal of Chromatography A 1218(27), 4078-4103.

Bakshi, S., He, Z.L. and Harris, W.G. (2014) A new method for separation, characterization, and quantification of natural nanoparticles from soils. Journal of Nanoparticle Research 16(2).

Baltrusaitis, J., Chen, H., Rubasinghege, G. and Grassian, V.H. (2012) Heterogeneous atmospheric chemistry of lead oxide particles with nitrogen dioxide increases lead solubility: environmental and health implications. Environmental Science & Technology 46(23), 12806-12813.

Boverhof, D.R., Bramante, C.M., Butala, J.H., Clancy, S.F., Lafranconi, M., West, J. and Gordon, S.C. (2015) Comparative assessment of nanomaterial definitions and safety evaluation considerations. Regulatory Toxicology and Pharmacology 73(1), 137-150.

Buffle, J. and Leppard, G.G. (1995) Characterization of aquatic colloids and macromolecules .1. Structure and behavior of colloidal material. Environmental Science & Technology 29(9), 2169-2175.

Buffle, J., Wilkinson, K.J., Stoll, S., Filella, M. and Zhang, J.W. (1998) A generalized description of aquatic colloidal interactions: The three-colloidal component approach. Environmental Science & Technology 32(19), 2887-2899.

Connor P.A. and McQuillan, A.J. (1999) Phosphate adsorption onto TiO₂ from aqueous solutions: An in situ internal reflection infrared spectroscopic study. Langmuir 15(8), 2916-2921.

Doetterl, S., Cornelis, J.T., Six, J., Bode, S., Opfergelt, S., Boeckx, P. and Van Oost, K. (2015) Soil redistribution and weathering controlling the fate of geochemical and physical carbon stabilization mechanisms in soils of an eroding landscape. Biogeosciences 12(5), 1357-1371.

Driver, S.J. and Perdue, E.M. (2014) Advances in the Physicochemical Characterization of Dissolved Organic Matter: Impact on Natural and Engineered Systems, pp. 75-86, American Chemical Society.

Dubascoux, S., Von Der Kammer, F., Le Hécho, I., Gautier, M.P. and Lespes, G. (2008) Optimisation of asymmetrical flow field flow fractionation for environmental nanoparticles separation. Journal of Chromatography A 1206(2), 160-165.

Furia, T.E. (1972) CRC handbook of food additives, CRC Press, Cleveland.

Gondikas, A.P., von der Kammer, F., Reed, R.B., Wagner, S., Ranville, J.F. and Hofmann, T. (2014) Release of TiO2 Nanoparticles from Sunscreens into Surface Waters: A One-Year Survey at the Old Danube Recreational Lake. Environmental Science & Technology 48(10), 5415-5422.

Hall, G.E.M., Vaive, J.E. and MacLaurin, A.I. (1996) Analytical aspects of the application of sodium pyrophosphate reagent in the specific extraction of the labile organic component of humus and soils. Journal of Geochemical Exploration 56(1), 23-36.

Hassellov, M., Readman, J.W., Ranville, J.F. and Tiede, K. (2008) Nanoparticle analysis and characterization methodologies in environmental risk assessment of engineered nanoparticles. Ecotoxicology 17(5), 344-361.

He, J.Z., De Cristofaro, A. and Violante, A. (1999) Comparison of adsorption of phosphate, tartrate, and oxalate on hydroxy aluminum montmorillonite complexes. Clays and Clay Minerals 47(2), 226-233.

Holland, H.D. and Turekian, K. (2010) Geochemistry of Earth Surface Systems: A derivative of the Treatise on Geochemistry, Academic Press.

Howard, A.G. (2010) On the challenge of quantifying man-made nanoparticles in the aquatic environment. Journal of Environmental Monitoring 12(1), 135-142.

Huang, P.M. and Sumner, M.E. (2011) Handbook of soil science: Properties and processes, CRC Press Taylor & Francis Group, Boca Raton.

Hui, H.A., Niu, Y.L., Zhao, Z.D., Hei, H.X. and Zhu, D.C. (2011) On the enigma of Nb-Ta and Zr-Hf fractionation-A critical review. Journal of Earth Science 22(1), 52-66.

ISO (2010) International Organization for Standardization. Nanotechnologies-vovabulary-part 1: Core Terms. ISO/TS 20004-1:2010.

Jolivet, J.P. (2000) Metal Oxide Chemistry and Synthesis: From Solution to Solid State, Wiley.

Labille, J., Harns, C., Bottero, J.Y. and Brant, J. (2015) Heteroaggregation of Titanium Dioxide Nanoparticles with Natural Clay Colloids. Environmental Science & Technology 49(11), 6608-6616.

Lawrence, C.R., Harden, J.W., Xu, X., Schulz, M.S. and Trumbore, S.E. (2015) Long-term controls on soil organic carbon with depth and time: A case study from the Cowlitz River Chronosequence, WA USA. Geoderma 247-248(Supplement C), 73-87.

Leppard, G.G., Buffle, J. and Baudat, R. (1986) A description of the aggregation properties of aquatic pedogenic fulvic acids: Combining physico-chemical data and microscopical observations. Water Research 20 (2), 185-196.

Lide, D.R. (2008) CRC Handbook of Chemistry and Physics, pp. 14–17, Taylor & Francis Group, Boca Raton, Florida.

Liu, Y.X., Li, Q.X., Ma, N., Sun, X.L., Bai, J.F. and Zhang, Q. (2014) Application of the Zr/Hf Ratio in the Determination of Hafnium in Geochemical Samples by High-Resolution Inductively Coupled Plasma Mass Spectrometry. Analytical Chemistry 86(23), 11570-11577.

Loeschner, K., Navratilova, J., Legros, S., Wagner, S., Grombe, R., Snell, J., von der Kammer, F., and Larsen, E. (2013) Optimisation and evaluation of asymmetrical flow field flow fractionation of silver nanoparticles. Journal of Chromatography A 1272(11), 116-125.

Loosli, F., Le Coustumer, P. and Stoll, S. (2013) TiO2 nanoparticles aggregation and disaggregation in presence of alginate and Suwannee River humic acids. pH and concentration effects on nanoparticle stability. Water Research 47(16), 6052-6063.

Loosli, F., Zebang, Y., Berti, D. and Baalousha, M. (2018) Toward a better extraction of titanium engineered nanomaterials from complex environmental matrices. NanoImpact 11, 119-127.

Loosli, F., Wang, J., Rothenberg, S., Bizimis, M., Winkler, C., Borovinskaya, O., Flamigni, L. and Baalousha, M. (2019) Sewage spills are a major source of engineered titanium dioxide release into the environment. Environmental Science: Nano 6(3), 763-777.

Montano, M.D., Lowry, G.V., von der Kammer, F., Blue, J. and Ranville, J.F. (2014) Current status and future direction for examining engineered nanoparticles in natural systems. Environmental Chemistry 11(4), 351-366.

Navratilova, J., Praetorius, A., Gondikas, A., Fabienke, W., von der Kammer, F. and Hofmann, T. (2015) Detection of Engineered Copper Nanoparticles in Soil Using Single Particle ICP-MS. International Journal of Environmental Research and Public Health 12(12), 15756-15768.

Neubauer, E., von der Kammer, F.D. and Hofmann, T. (2013) Using FLOWFFF and HPSEC to determine trace metal colloid associations in wetland runoff. Water Research 47(8), 2757-2769.

Pansu, M. and Gautheyrou, J. (2006) Handbook of Soil Analysis - Mineralogical, Organic and Inorganic Methods, Springer.

Philippe, A. and Schaumann, G.E. (2014) Interactions of Dissolved Organic Matter with Natural and Engineered Inorganic Colloids: A Review. Environmental Science & Technology 48(16), 8946-8962.

Post, J.E. (1999) Manganese oxide minerals: Crystal structures and economic and environmental significance. Proceedings of the National Academy of Sciences 96(7), 3447-3454.

Praetorius, A., Labille, J., Scheringer, M., Thill, A., Hungerbuehler, K. and Bottero, J.-Y. (2014) Heteroaggregation of Titanium Dioxide Nanoparticles with Model Natural Colloids under Environmentally Relevant Conditions. Environmental Science & Technology 48(18), 10690-10698.

Pronk, G.J., Heister, K. and Kogel-Knabner, I. (2011) Iron Oxides as Major Available Interface Component in Loamy Arable Topsoils. Soil Science Society of America Journal 75(6), 2158-2168.

Regelink, I.C., Voegelin, A., Weng, L.P., Koopmans, G.F. and Comans, R.N.J. (2014) Characterization of Colloidal Fe from Soils Using Field-Flow Fractionation and Fe K-Edge X-ray Absorption Spectroscopy. Environmental Science & Technology 48(8), 4307-4316.

Regelink, I.C., Weng, L., Koopmans, G.F. and Van Riemsdijk, W.H. (2013) Asymmetric flow field-flow fractionation as a new approach to analyse iron-(hydr)oxide nanoparticles in soil extracts. Geoderma 202, 134-141.

Schwertfeger, D.M., Velicogna, J.R., Jesmer, A.H., Saatcioglu, S., McShane, H., Scroggins, R.P. and Princz, J.I. (2017) Extracting Metallic Nanoparticles from Soils for Quantitative Analysis: Method Development Using Engineered Silver Nanoparticles and SP-ICP-MS. Analytical Chemistry 89(4), 2505-2513.

Sharma, V.K., Filip, J., Zboril, R. and Varma, R.S. (2015) Natural inorganic nanoparticles - formation, fate, and toxicity in the environment. Chemical Society Reviews 44(23), 8410-8423.

Simoes, M.C., Hughes, K.J., Ingham, D.B., Ma, L. and Pourkashanian, M. (2017) Estimation of the Thermochemical Radii and Ionic Volumes of Complex Ions. Inorganic Chemistry 56(13), 7566-7573.

Tang, Z.Y., Wu, L.H., Luo, Y.M. and Christie, P. (2009) Size fractionation and characterization of nanocolloidal particles in soils. Environmental Geochemistry and Health 31(1), 1-10.

Tatzber, M., Stemmer, M., Splegel, H., Katziberger, C., Haberhauer, G., Mentler, A. and Gerzabek, M.H. (2007) FTIR-spectroscopic characterization of humic acids and humin fractions obtained by advanced NaOH, Na4P2O7, and Na2CO3 extraction procedures. Journal of Plant Nutrition and Soil Science-Zeitschrift Fur Pflanzenernahrung Und Bodenkunde 170(4), 522-529.

Therezien, M., Thill, A. and Wiesner, M.R. (2014) Importance of heterogeneous aggregation for NP fate in natural and engineered systems. Science of the Total Environment 485–486(0), 309-318.

Tiede, K., Boxall, A.B.A., Tear, S.P., Lewis, J., David, H. and Hassellov, M. (2008) Detection and characterization of engineered nanoparticles in food and the environment. Food Additives and Contaminants Part a-Chemistry Analysis Control Exposure & Risk Assessment 25(7), 795-821.

Tuoriniemi, J., Cornelis, G. and Hassellov, M. (2014) Improving the accuracy of single particle ICPMS for measurement of size distributions and number concentrations of nanoparticles by determining analyte partitioning during nebulisation. Journal of Analytical Atomic Spectrometry 29(4), 743-752.

Wagner, S., Gondikas, A., Neubauer, E., Hofmann, T. and von der Kammer, F. (2014) Spot the Difference: Engineered and Natural Nanoparticles in the Environment-Release, Behavior, and Fate. Angewandte Chemie-International Edition 53(46), 12398-12419.

Wang, H.T., Adeleye, A.S., Huang, Y.X., Li, F.T. and Keller, A.A. (2015) Heteroaggregation of nanoparticles with biocolloids and geocolloids. Advances in Colloid and Interface Science 226, 24-36.

Weinberg, H., Galyean, A. and Leopold, M. (2011) Evaluating engineered nanoparticles in natural waters. Trac-Trends in Analytical Chemistry 30(1), 72-83.

Wigginton, N.S., Haus, K.L. and Hochella, M.F. (2007) Aquatic environmental nanoparticles. Journal of Environmental Monitoring 9(12), 1306-1316.

Wilkinson, K.J., Joz-Roland, A. and Buffle, J. (1997) Different roles of pedogenic fulvic acids and aquagenic biopolymers on colloid aggregation and stability in freshwaters. Limnology and Oceanography 42(8), 1714-1724.

Wilkinson, K.J., Balnois, E., Leppard, G.G. and Buffle, J. (1999) Characteristic features of the major components of freshwater colloidal organic matter revealed by transmission electron and atomic force microscopy. Colloids and Surface A: Physicochemical and Engineering Aspects 155 (2-3), 287-310.

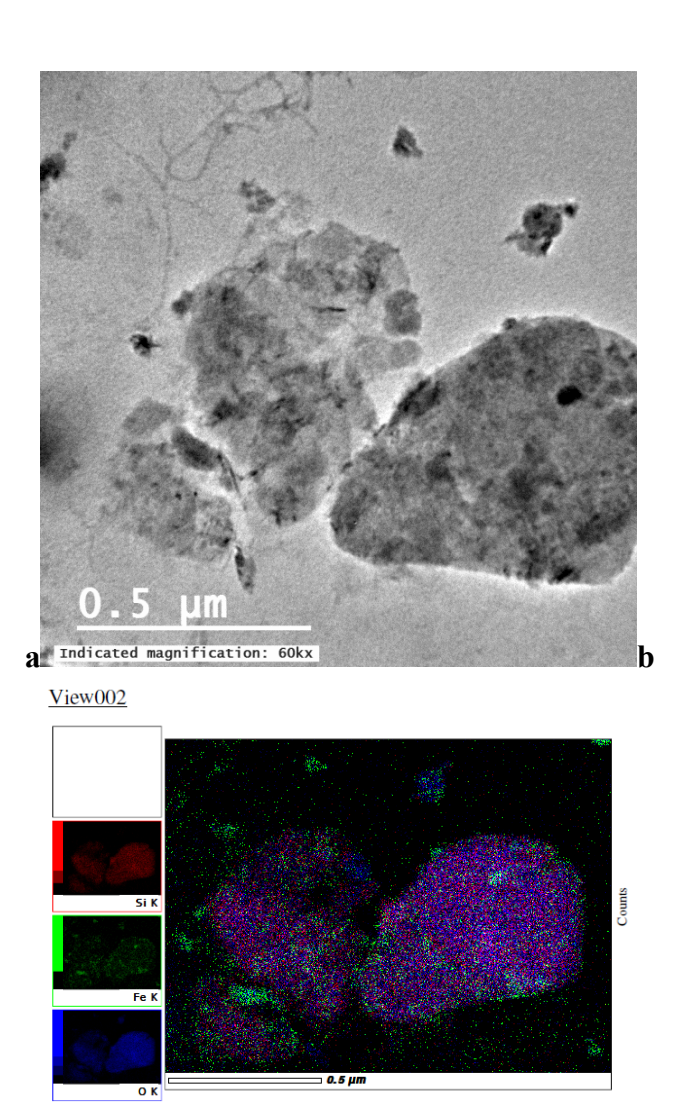
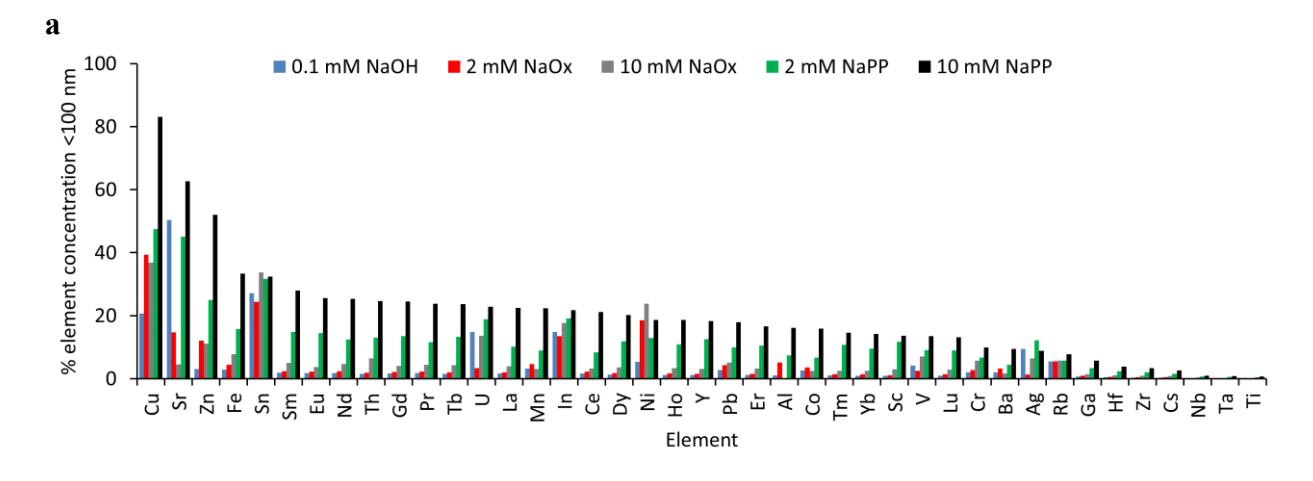


Figure 1. Transmission electron microscopy (TEM) micrographs of natural nanomaterial (NMM) heteroaggregates from (a) Stoop Creek and (b) X-EDS map of a. In the X-EDS map, Si, Fe, and O are indicated by the red, green and blue colors, respectively. Scale bar corresponds to $0.5~\mu m$.



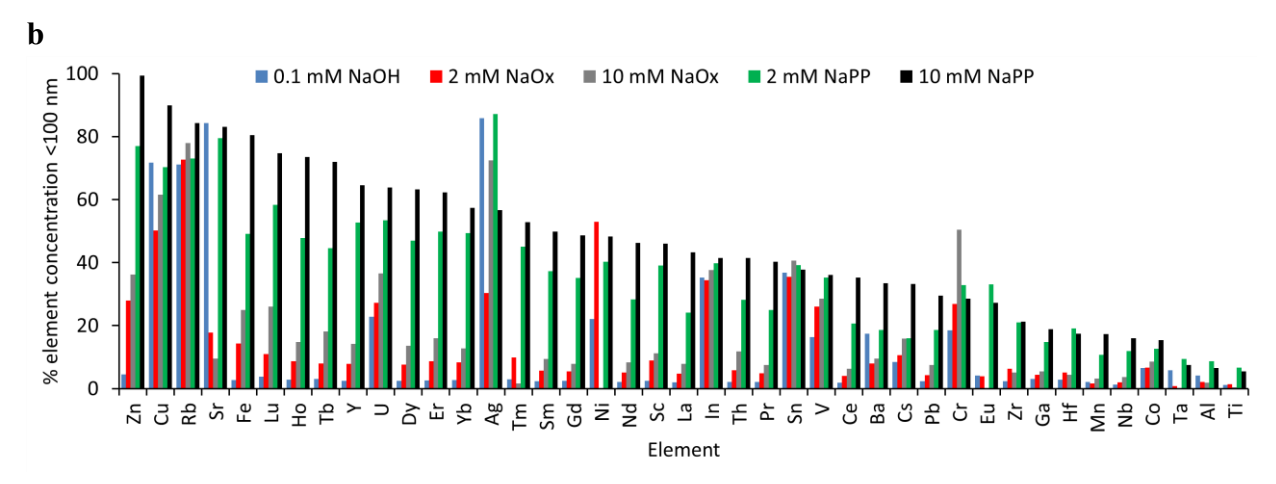
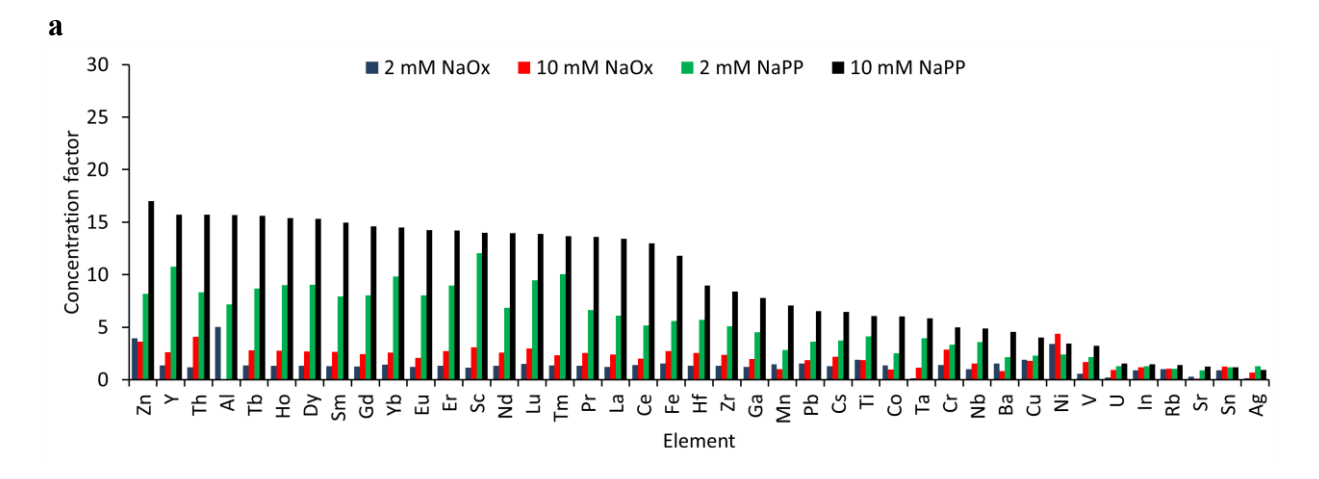


Figure 2. Percentage of element concentrations in the extracted NNM suspensions compared to their concentrations in the bulk waters: (a) Stoop Creek, and (b) Crane Creek. Elements are ordered from highest to lowest fraction in the 10 mM NaPP-extracted NNM suspensions.



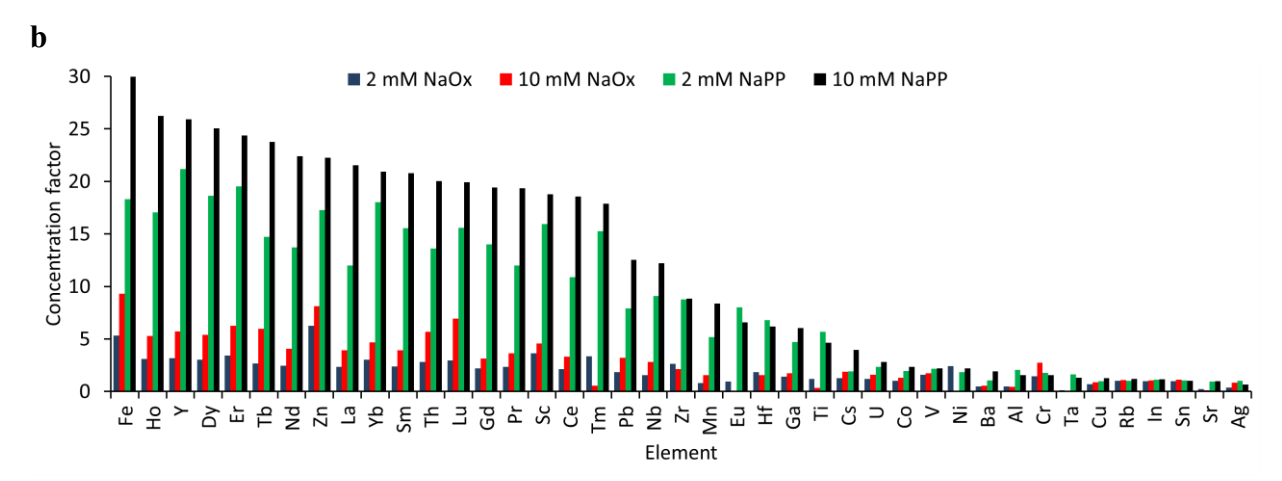
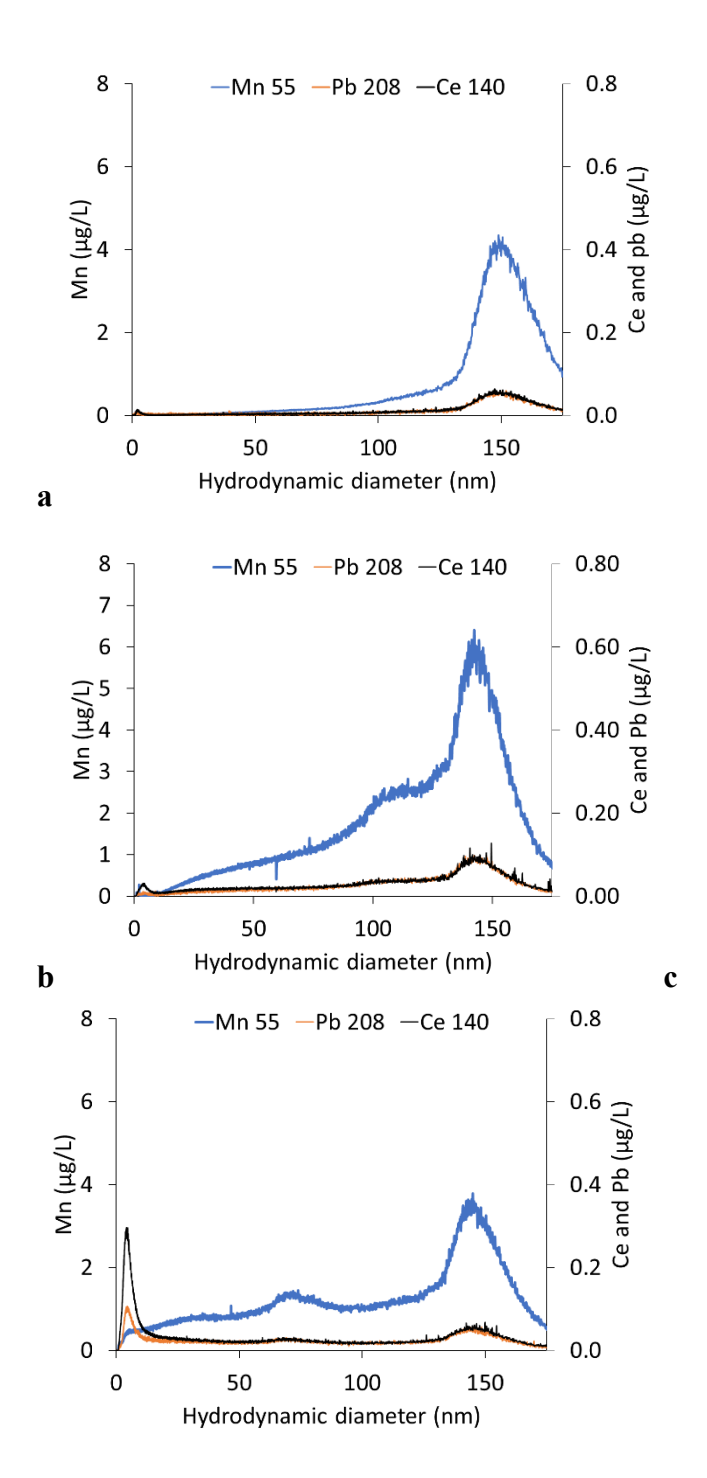


Figure 3. Elemental concentration factor which represent the element concentration in NaOx-and NaPP-extracted NNMs compared to the corresponding element concentration in the 0.1 mM NaOH-extracted NNMs for (a) Stoop Creek and (b) Crane Creek. Elements are ordered from highest to lowest concentration factor for each sample.



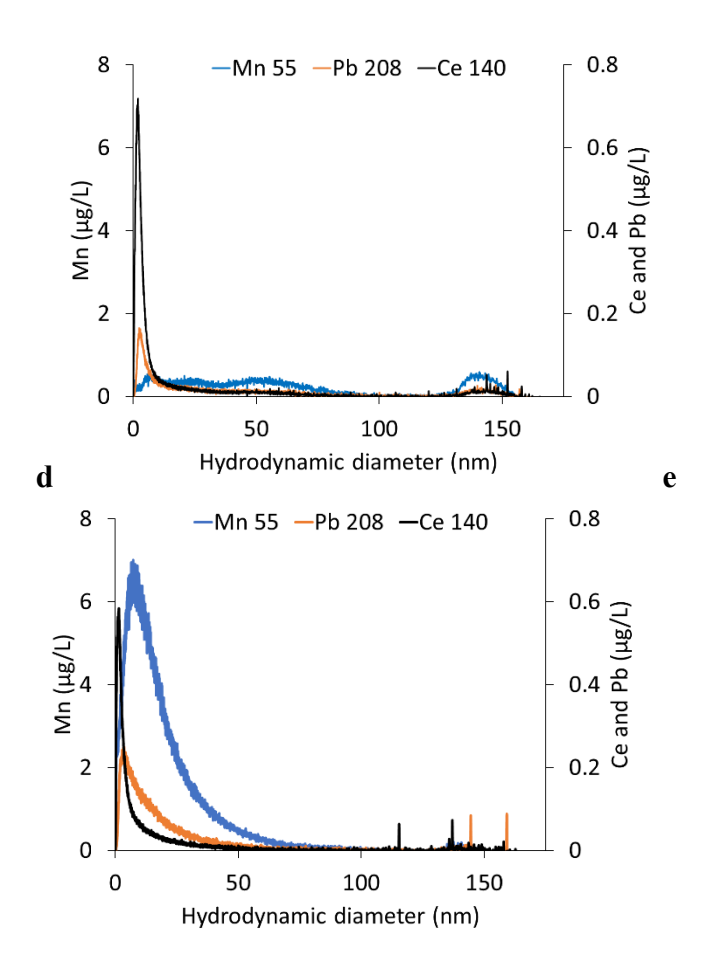
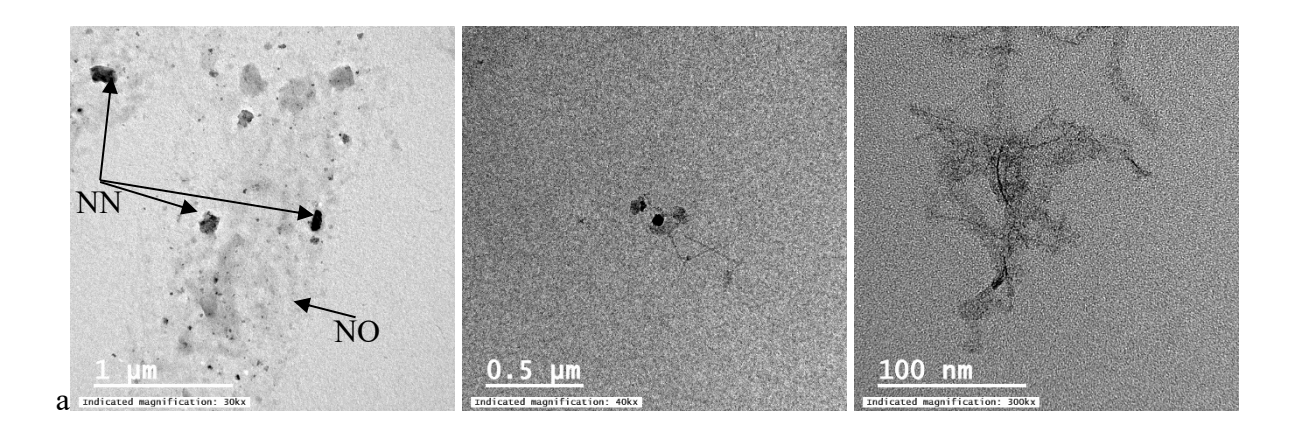


Figure 4. Effect of extractant on extracted NNM size distribution for Stoop Creek. Typical flow-field flow fractionations fractograms of (a) 0.1 mM NaOH-, (b) 2 mM NaOx-, (c) 10 mM NaOx-, (d) 2 mM NaPP-, and (e) 10 mM NaPP- extracted NNMs. Mn, Ce, and Pb are used as examples and other elements are presented in the SI section (Figure S2). AF4 conditions: channel flow of 1.0 mL min⁻¹, gradient cross flow from 2.5 to 0 mL min⁻¹ over 45 minutes. Size distributions for NNMs extracted from Crane Creek water are presented in the SI section (Figures S1 and S3).



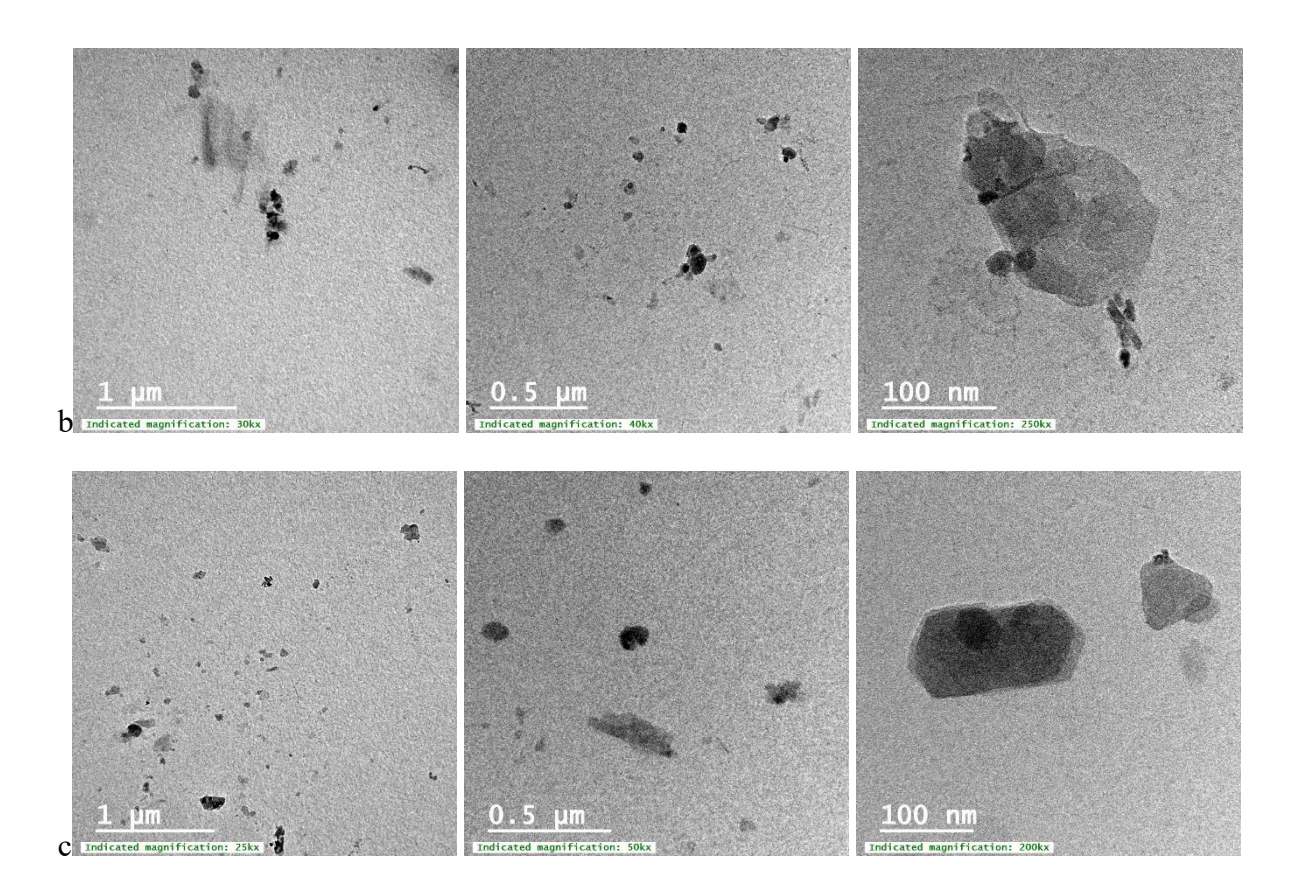


Figure 5. Typical TEM micrographs of (a) 0.1 mM NaOH-, (b) 10 mM NaOx-, and (c) 10 mM NaPP-extracted NNMs from Stoop Creek water.

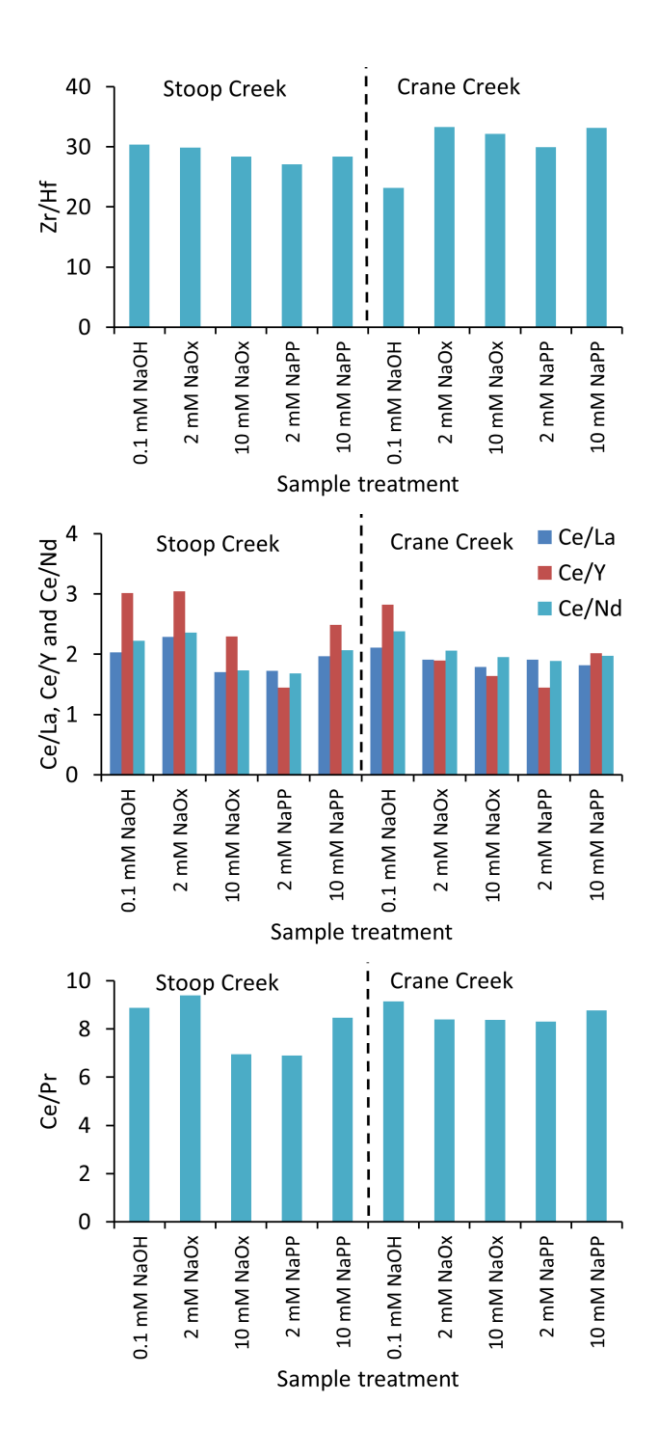


Figure 6. Elemental ratios calculated from total elemental concentrations of the extracted NNM suspensions as a function of extractant for: (a) Zr/Hf, (b) Ce/La, Ce/Y, and Ce/Nd, (c) Ce/Pr.

Table S1. Metal concentration in the bulk sample. All samples were digested using HF: HNO₃ (3:1)

Element	Stoop Creek element concentration	Crane Creek element concentration				
Dienient	$(\mu g L^{-1})$	(μg L ⁻¹)				
Rb85	87.7	6.95				
Sr88	191.1	42.70				
Y89	18.6	0.69				
Zr90	140.5	3.58				
Nb93	15.2	0.29				
Ag107	0.74	0.02				
Cd111	0.34	0.028				
In115	0.06	0.026				
Sn118	13.4	11.46				
Cs133	4.51	0.11				
Ba137	367.8	52.85				
La139	19.26	1.14				
Ce140	40.24	2.54				
Pr141	4.22	0.25				
Nd146	16.21	0.98				
Sm149	3.12	0.19				
Eu151	0.74	0.05				
Gd157	3.38	0.19				
Tb159	0.54	0.025				
Dy163	3.29	0.129				
Ho165	0.68	0.025				

Er167	2.03	0.07
Tm169	0.30	0.01
Yb173	2.07	0.07
Lu175	0.30	0.01
Hf178	4.24	0.13
Ta181	2.80	0.04
Pb208	30.47	1.83
Th232	7.55	0.33
U238	2.02	0.09
Al27	45746	4265
Sc45	11.17	0.34
Ti47	5841.1	100.7
V51	78.09	2.36
Cr53	40.26	2.05
Mn55	1952.7	425.7
Fe57	20781	1685
Co59	18.50	1.71
Ni60	14.18	1.26
Cu63	130.07	2.77
Zn66	86.92	16.25
Ga69	12.14	0.44

Table S2. Elemental concentration ($\mu g L^{-1}$) in the extracted NNM suspensions. All samples were digested using HF: HNO₃ (3:1).

		Sto	oop Cre	ek	Crane creek						
	0.1 mM NaOH	2 mM NaOx	10 mM NaOx	2 mM NaPP	10 mM NaPP	0.1 mM NaOH	2 mM NaOx	10 mM NaOx	2 mM NaPP	10 mM NaPP	
Rb85	4.85	4.78	4.99	4.98	6.85	4.94	5.05	5.41	5.08	5.86	
Sr88	96.30	28.10	8.70	86.20	119.70	36.00	7.60	4.10	33.90	35.50	
Y89	0.22	0.30	0.57	2.34	3.42	0.02	0.05	0.10	0.36	0.44	
Zr90	0.55	0.73	1.31	2.80	4.63	0.09	0.23	0.18	0.75	0.76	
Nb93	0.03	0.03	0.05	0.11	0.15	0.00	0.01	0.01	0.03	0.05	
Ag107	0.07	0.01	0.05	0.09	0.07	0.02	0.01	0.02	0.02	0.01	
Cd111	0.01	0.01	0.01	0.07	0.09	0.00	0.00	0.00	0.01	0.00	
In115	0.01	0.01	0.01	0.01	0.01	0.01	0.01	0.01	0.01	0.01	
Sn118	3.64	3.28	4.52	4.25	4.35	4.21	4.07	4.66	4.49	4.33	
Cs133	0.02	0.02	0.04	0.07	0.12	0.01	0.01	0.02	0.02	0.04	
Ba137	7.64	11.84	6.25	16.38	34.69	9.23	4.22	5.01	9.82	17.68	
La139	0.32	0.40	0.77	1.96	4.33	0.02	0.05	0.09	0.27	0.49	
Ce140	0.66	0.91	1.31	3.38	8.50	0.05	0.10	0.16	0.53	0.90	
Pr141	0.07	0.10	0.19	0.49	1.00	0.01	0.01	0.02	0.06	0.10	
Nd146	0.29	0.39	0.76	2.01	4.11	0.02	0.05	0.08	0.28	0.45	
Sm149	0.06	0.08	0.16	0.46	0.87	0.00	0.01	0.02	0.07	0.09	
Eu151	0.01	0.02	0.03	0.11	0.19	0.00	0.00	0.00	0.02	0.01	
Gd157	0.06	0.07	0.14	0.46	0.83	0.01	0.01	0.02	0.07	0.09	
Tb159	0.01	0.01	0.02	0.07	0.13	0.00	0.00	0.01	0.01	0.02	
Dy163	0.04	0.06	0.12	0.39	0.66	0.00	0.01	0.02	0.06	0.08	
Ho165	0.01	0.01	0.02	0.07	0.13	0.00	0.00	0.00	0.01	0.02	
Er167	0.02	0.03	0.07	0.21	0.34	0.00	0.01	0.01	0.03	0.04	

Tm169	0.00	0.00	0.01	0.03	0.04	0.00	0.00	0.00	0.01	0.01
Yb173	0.02	0.03	0.05	0.20	0.29	0.00	0.01	0.01	0.03	0.04
Lu175	0.00	0.00	0.01	0.03	0.04	0.00	0.00	0.00	0.01	0.01
Hf178	0.02	0.02	0.05	0.10	0.16	0.00	0.01	0.01	0.03	0.02
Ta181	0.00	0.00	0.01	0.02	0.02	0.00	0.00	0.00	0.00	0.00
Pb208	0.84	1.30	1.56	3.03	5.47	0.04	0.08	0.14	0.34	0.54
Th232	0.12	0.14	0.48	0.98	1.86	0.01	0.02	0.04	0.09	0.14
U238	0.30	0.07	0.28	0.38	0.46	0.02	0.02	0.03	0.05	0.06
Al27	470	2364	30230	3376	7374	179	88	80	369	278
Sc45	0.11	0.12	0.33	1.31	1.52	0.01	0.03	0.04	0.13	0.15
Ti47	7.40	13.90	13.60	30.50	44.90	1.20	1.40	0.40	6.70	5.50
V51	3.29	1.92	5.48	7.13	10.58	0.39	0.61	0.67	0.83	0.85
Cr53	0.80	1.12	2.30	2.68	3.97	0.38	0.55	1.04	0.67	0.59
Mn55	61.80	90.20	61.30	175.50	437.20	8.80	6.90	13.60	45.60	73.50
Fe57	588	910	160	3288	6945	45	240	421	828	1356
Co59	0.49	0.66	0.47	1.23	2.94	0.11	0.11	0.15	0.22	0.26
Ni60	0.77	2.63	3.37	1.84	2.64	0.28	0.67	3.01	0.51	0.61
Cu63	26.95	51.24	47.86	61.75	108.14	1.99	1.39	1.71	1.95	2.49
Zn66	2.66	10.51	9.66	21.75	45.22	0.73	4.54	5.88	12.51	16.13
Ga69	0.09	0.11	0.18	0.40	0.70	0.01	0.02	0.02	0.07	0.08

Table S3. Elemental ratios.

			Sto	oop Cre	ek	Crane creek						
	Bulk	NaOH	2 mM NaOx	10 mM NaOx	2 mM NaPP	10 mM NaPP	Bulk	NaOH	2 mM NaOx	10 mM NaOx	2 mM NaPP	10 mM NaPP
Zr/Hf	33.1	30.6	30.2	28.4	27.2	28.4	27.3	21.5	32.1	30.7	30.1	33.0
Ce/La	2.1	2.0	2.3	1.7	1.7	2.0	2.2	2.1	1.9	1.8	1.9	1.8
Ce/Pr	9.5	8.9	9.4	7.0	6.9	8.5	10.0	9.6	8.6	8.4	8.3	8.8
Ce/Nd	2.5	2.2	2.4	1.7	1.7	2.1	2.6	2.4	2.1	2.0	1.9	2.0
Ti/Nb	383.5	238.7	448.4	289.4	274.8	299.3	349.7	300.0	233.3	36.4	197.1	119.6

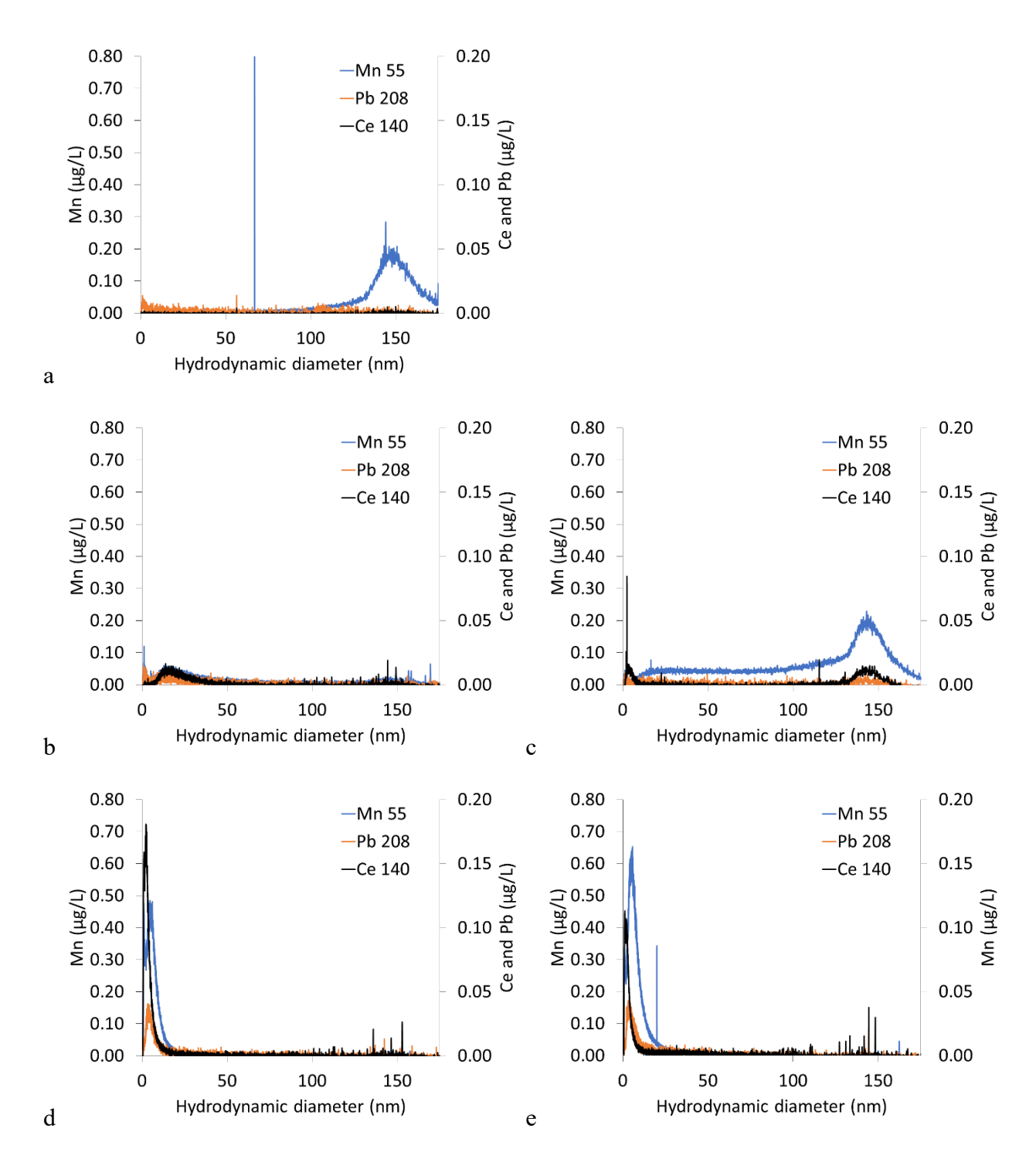
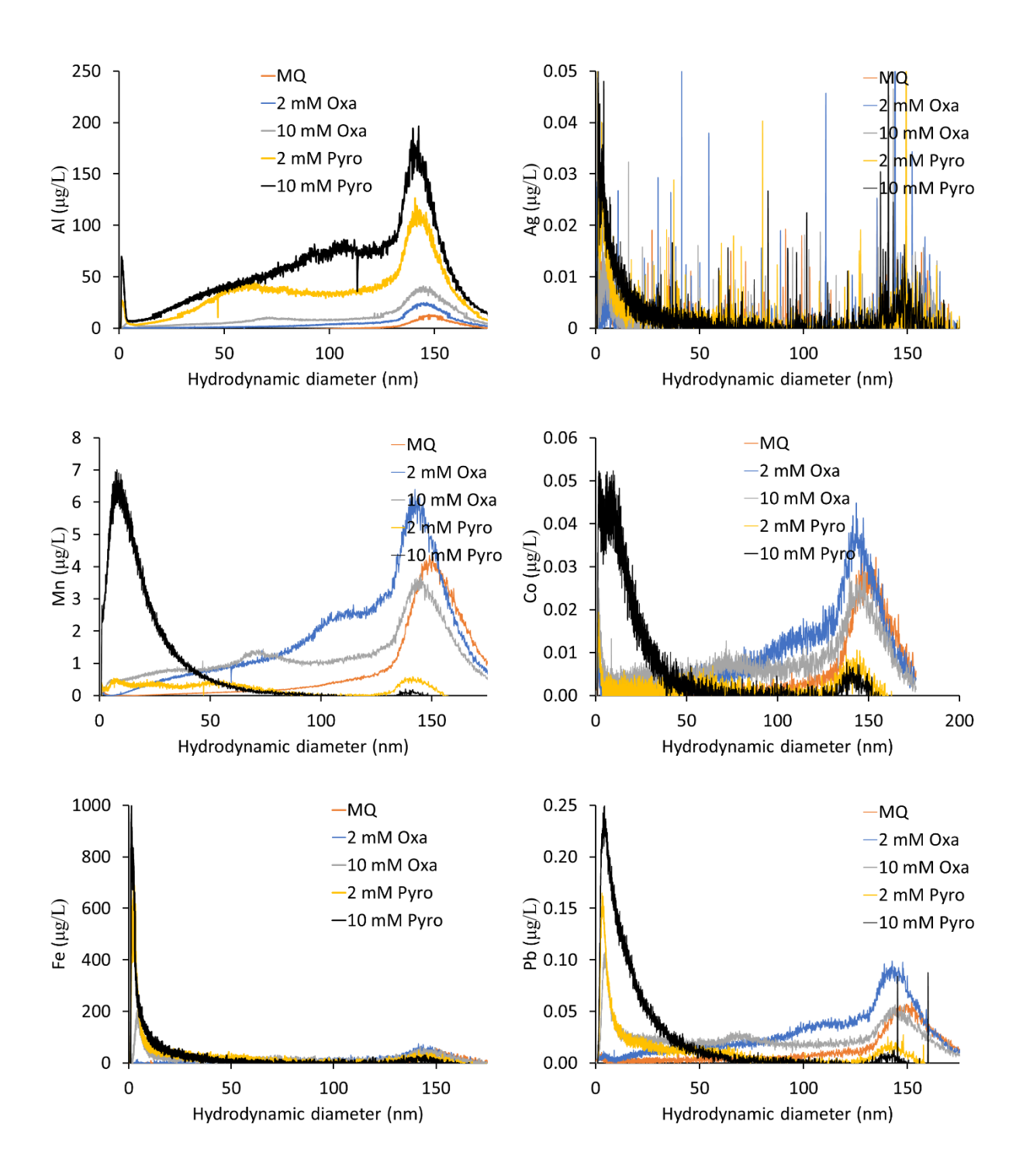


Figure S1. Effect of extractant on natural nanoparticle (NNM) size distribution in Crane Creek water. Typical flow-field flow fractionations fractograms (a) 0.1 mM NaOH-, (b) 2 mM NaOx-, (c) 10 mM NaOx-, (d) 2 mM NaPP-, and (e) 10 mM NaPP-extracted NNMs. Mn, Ce, and Pb are illustrated as examples in the figure. Data on other metals are presented in the supplementary information (Figure S3).

Journal of Beijing University of Posts And Telecommunications ISSN: 1007-5321 Impact Factor: 6.2



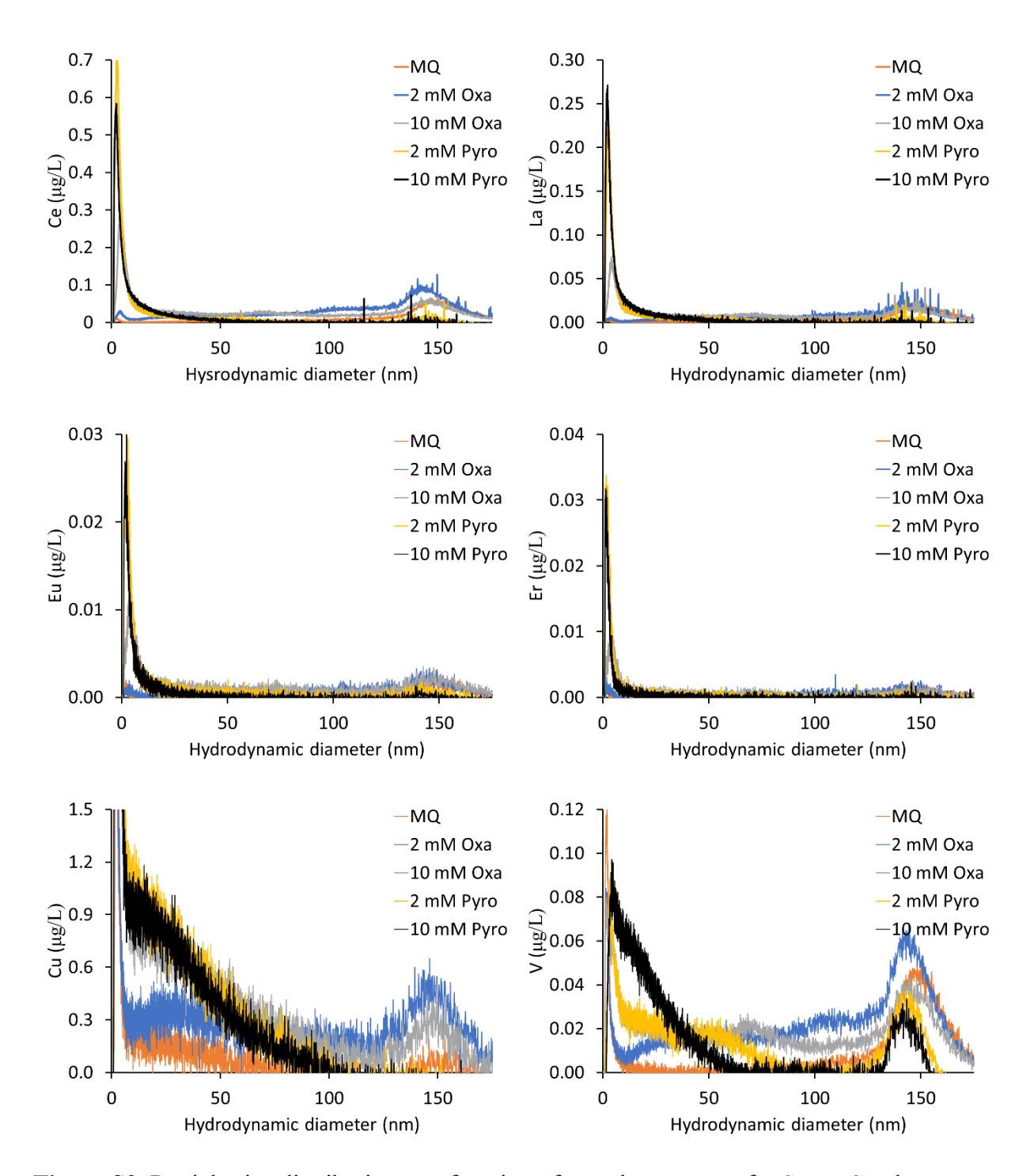
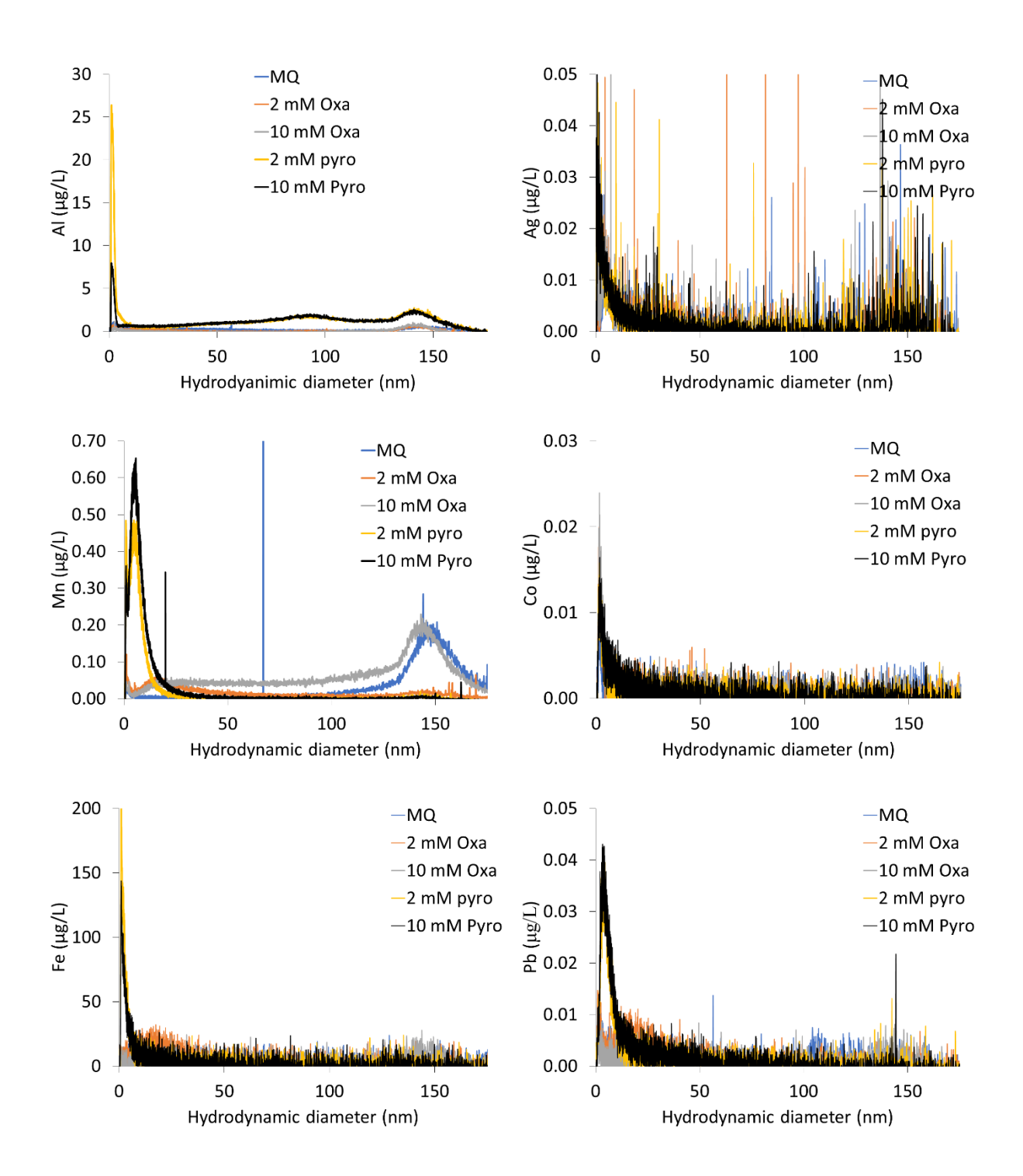


Figure S2. Particle size distribution as a function of sample treatment for Stoop Creek water. AF4 conditions: channel flow of 1.0 ml min⁻¹, gradient cross flow from 2.5 to 0 ml min⁻¹ over 45 minutes.



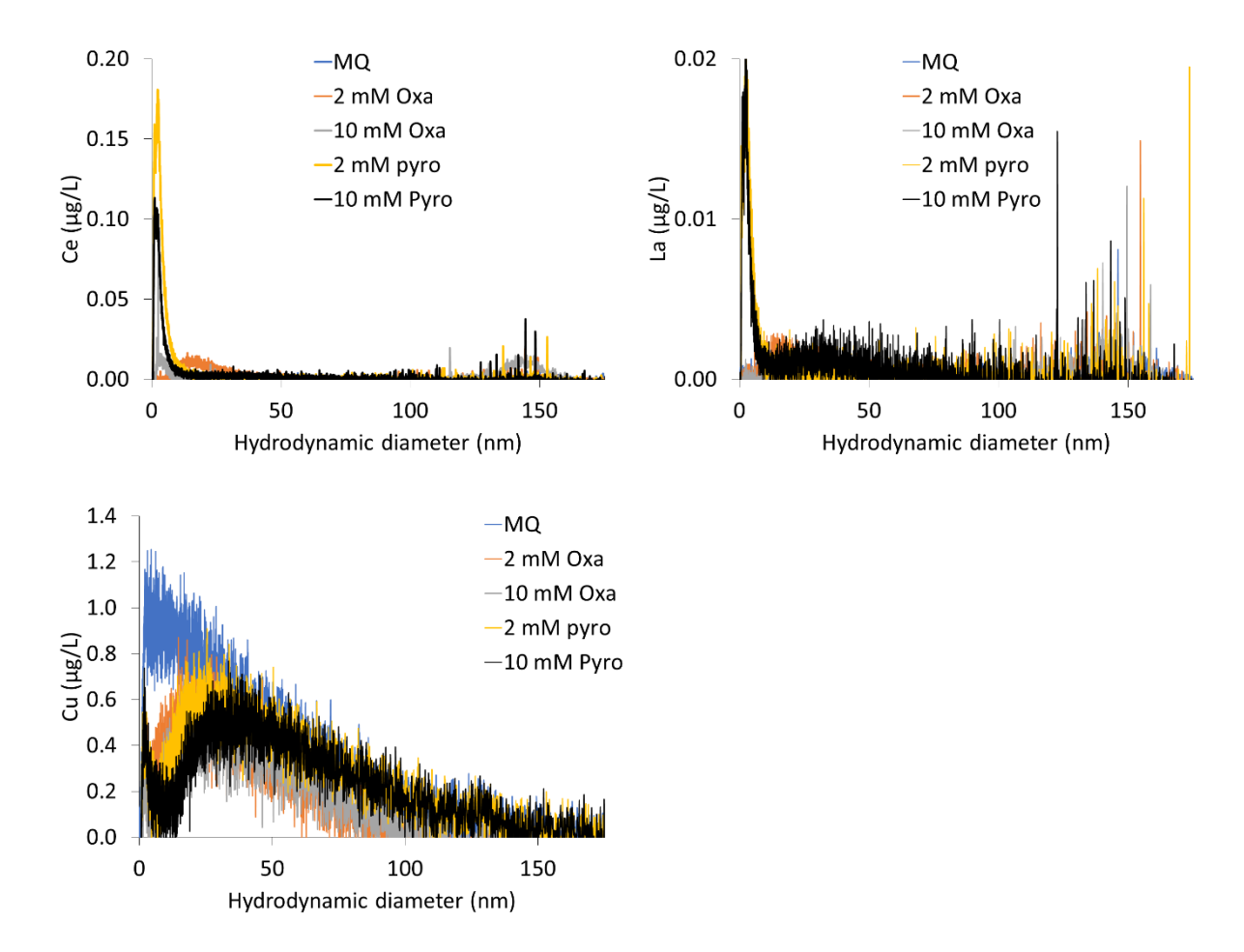


Figure S3. Particle size distribution as a function of sample treatment for Crane Creek water. AF4 conditions: channel flow of 1.0 ml min⁻¹, gradient cross flow from 2.5 to 0 ml min⁻¹ over 45 minutes.

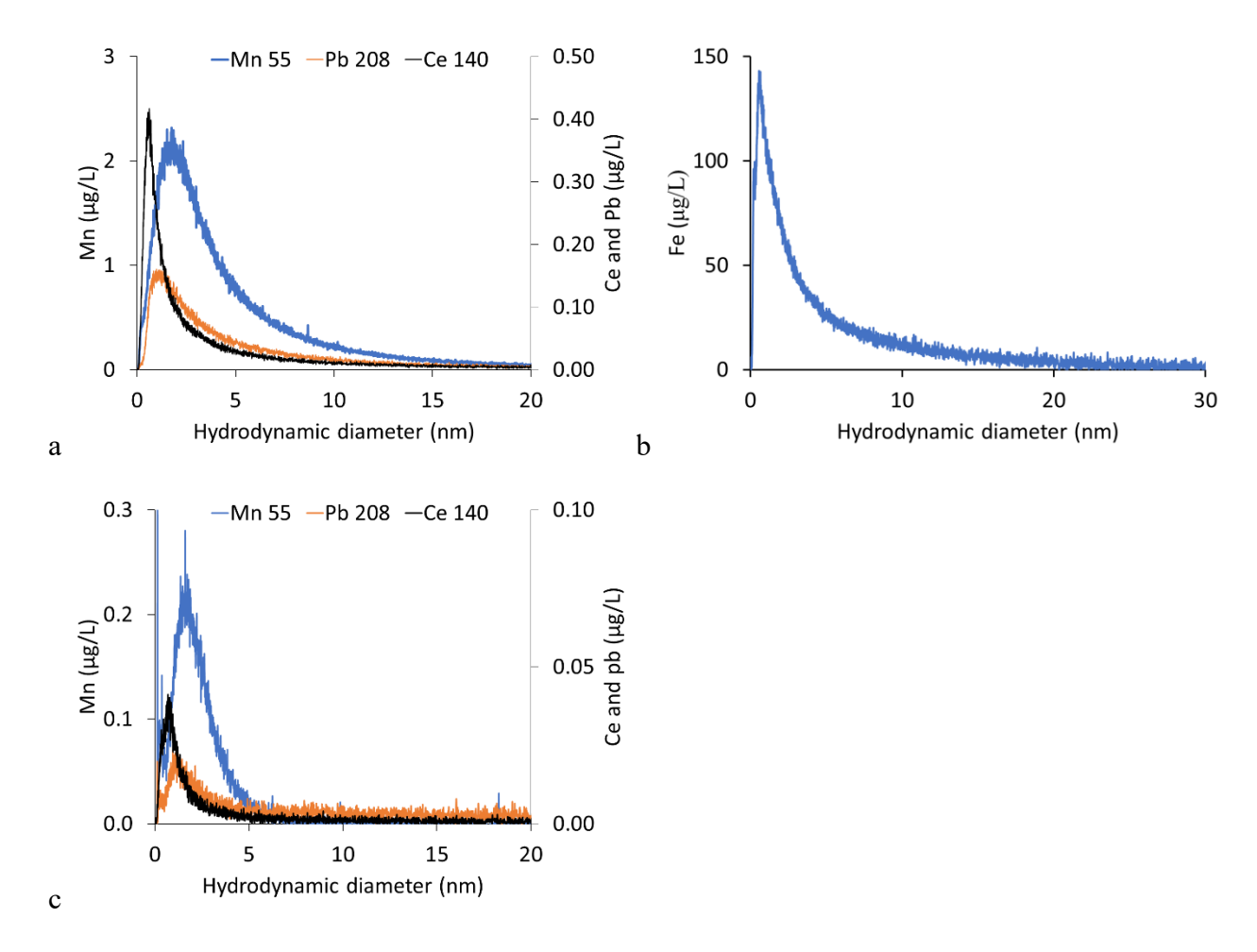


Figure S4. Particle size distribution as a function of sample treatment for Stoop Creek (a and b) and Crane Creek (c). AF4 conditions: channel flow of 1.0 ml min⁻¹, gradient cross flow from 4 to 0 ml min⁻¹ over 120 minutes.

Journal of Beijing University of Posts And Telecommunications ISSN: 1007-5321 Impact Factor: 6.2

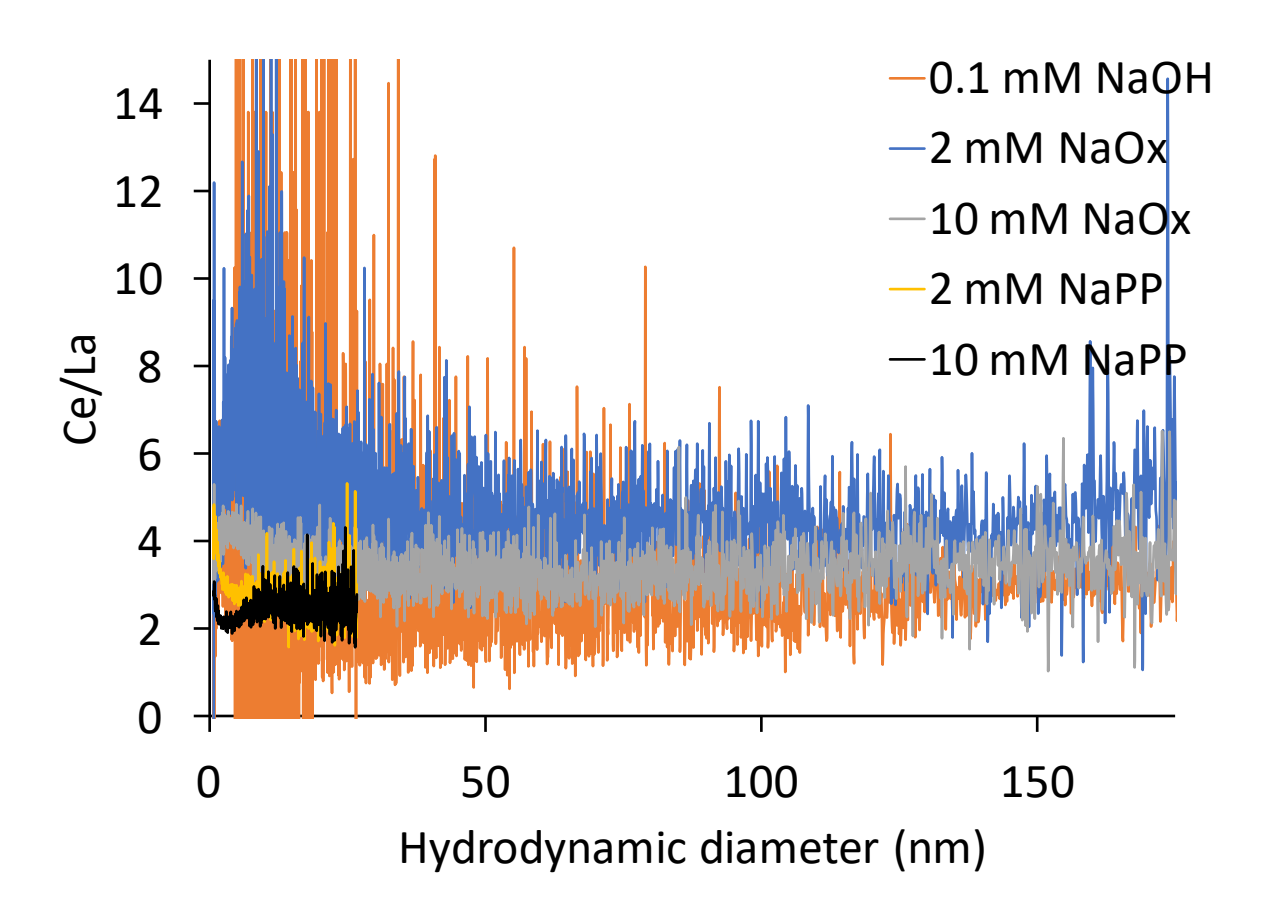


Figure S5. Ce/La as a function of the NNM extraction protocol.

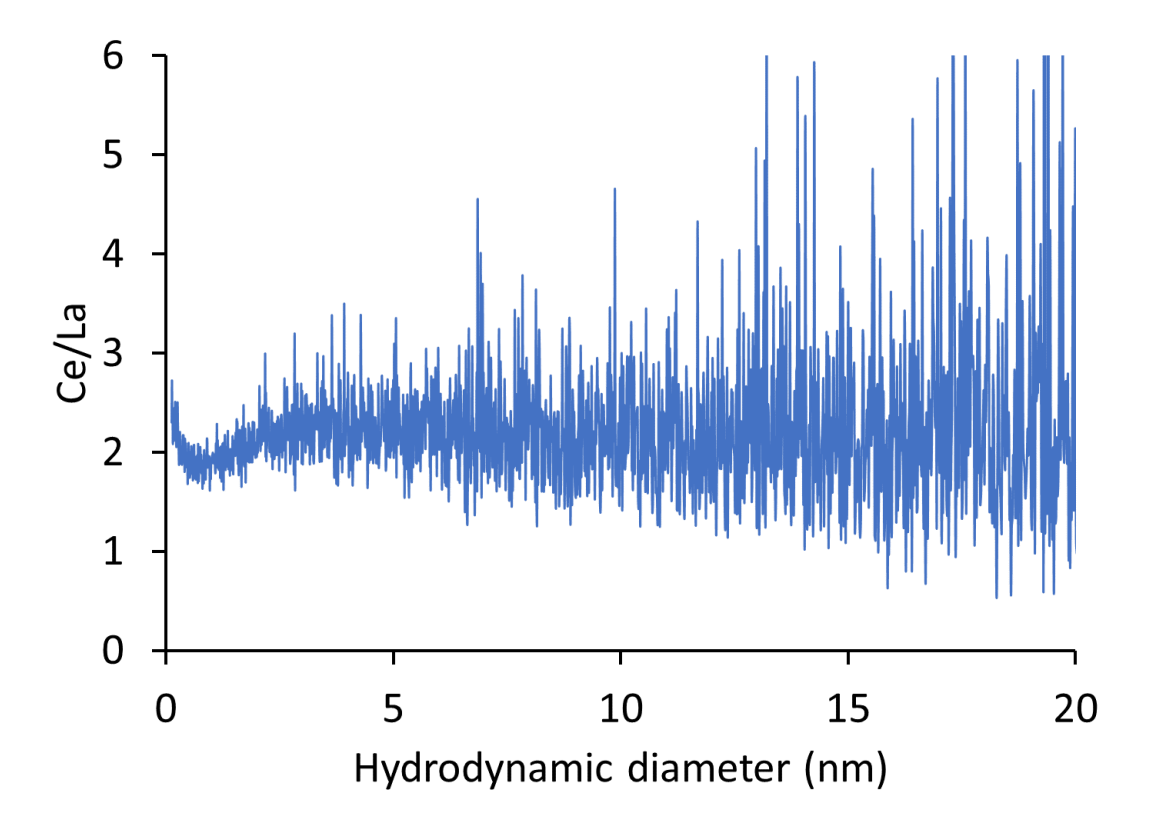


Figure S6. Ce/La ratio as a function of size for Stoop Creek water. AF4 conditions: channel flow of 1.0 ml min⁻¹, gradient cross flow from 4 to 0 ml min⁻¹ over 120 minutes.